Journal of the Meteorological Society of Japan

EARLY ONLINE RELEASE

The DOI for this manuscript is
DOI:10.2151/jmsj.2021-035
J-STAGE Advance published date: March 12th, 2021
The final manuscript after publication will replace the preliminary version at the above DOI once it is available.

Progress From TRMM To GPM

Kenji NAKAMURA[1]

Dokkyo University, Saitama, Japan

August 4, 2020
December 4, 2020
January 16, 2021

----

1) Corresponding author: Kenji Nakamura, Dokkyo University, 1-1, Gakuencho, Soka, Saitama 340-0042 JAPAN.
Email: k13002@dokkyo.ac.jp

Abstract

The Tropical Rainfall Measuring Mission (TRMM) satellite was launched in 1997 and the observations continued for more than 17 years. The features of TRMM observation were as follows: (a) it followed a non-sun synchronized orbit that enabled diurnal variation of precipitation to be investigated, (b) it carried a precipitation radar and microwave and infrared radiometers, along with two instruments of opportunity in the form of a lighting sensor and a radiation budget sensor, and (c) it worked as a standard reference for precipitation measurements for other spaceborne microwave radiometers, which enabled global rain maps to be developed. For science, TRMM provided precise and accurate rain distributions over tropical and subtropical regions. The rainfall results are primarily important for the study of the precipitation climatologies, while the three-dimensional images of precipitation systems enabled the study of the global characteristics of precipitation systems. Technologically, the spaceborne rain radar onboard TRMM demonstrated the effectiveness of radars in space, while the combination with other rain observation instruments showed its effectiveness as a calibration source. Multi-satellite rain maps in which TRMM was the reference standard have been developed, and they became prototypes of the multi-satellite Earth observation systems. Based on the great success of TRMM, the Global Precipitation

Measurement (GPM) was designed to expand TRMM’s coverage to higher latitudes. The core satellite of GPM is equipped with a dual frequency precipitation radar (DPR) and a microwave radiometer. DPR consists of a Ku-band radar (KuPR) and a Ka-band radar (KaPR) and has a capability to discriminate solid from liquid precipitation. The period of the precipitation measurement with spaceborne radars extended to more than 23 years which may make it possible to detect the change of precipitation climatology related to change in the global environment. While TRMM’s and GPM’s accomplishments are very broad, this paper tries to highlight Japan’s contributions to the science of these missions.

Keywords TRMM, GPM, Precipitation, Satellite, radar, radiometer, global rain map

1. Introduction

The Earth system, ecosystems, and human society critically depend on precipitation. Rain is traditionally measured using ground-based rain gauges; however, it is difficult to make accurate measurements of precipitation because of its significant spatial and temporal variations. Developed countries have established wide and dense rain gauge networks and good radar networks. For example, Japan operates a few thousand rain gauges and a few tens of rain radars, but many countries have poor precipitation measurement networks. In addition, vast ocean areas, tropical rain forests, and high mountain regions lack extensive networks (Kidd et al. 2017). Precipitation measurements from space are thus a viable alternative for precipitation measurement.

The first spaceborne microwave radiometer for Earth observation was launched by the Soviet Union in 1968 onboard COSMOS-243. In the 1970s, the US pioneered precipitation measurement from space using microwave radiometers, such as the Electrically Scanning Microwave Radiometer (ESMR) onboard NUMBUS-5 and the Scanning Multichannel Microwave Radiometer (SMMR) onboard NUMBUS-7 (e.g., Wilheit et al. 1976; Wilheit et al. 1977; Wilheit and Chang 1980). However, the accuracy obtained was insufficient, and the microwave radiometer had difficulty in mapping rain distribution over lands. The use of spaceborne rain radar was then considered to be a strong and promising alternative. A workshop entitled “Precipitation Measurements from Space” organized by the National Aeronautics and Space Administration (NASA) and the National

Oceanic and Atmospheric Administration (NOAA) was held in the US in 1981 to encourage NASA's headquarters to initiate a new precipitation measurement program. In this workshop, visible/infrared (VIS/IR) and microwave passive techniques were discussed, and the necessity of employing a spaceborne radar was recognized. The workshop summary concisely and accurately described the status of precipitation measurements in that era as follows (Atlas and Thiele 1981):

The measurement of precipitation from space on a global scale is a formidable problem because as yet there are no guaranteed methods which can be relied upon to perform under all circumstances around the world. Nevertheless, we already have some VIS and IR techniques that provide climatologically useful data in the subtropical belt. Also, over the oceans we are quite confident that these methods can be extended to extratropical regions by means of improved microwave radiometers. The use of combinations of measurement systems should be most valuable in filling the great gaps in our knowledge of oceanic precipitation, and it would serve a broad spectrum of users both in climate research and global weather prediction.

Furthermore, for the first time, we now have a set of conceptual methods including spaceborne radar, either by itself or as part of a hybrid system, which show promise of operating over both land and ocean. At the very least, these approaches deserve serious feasibility studies and field trials. In short, the needs have been well articulated and the *technology is within reach. Therefore, it is time to proceed with a strong and well-ordered program of study and development as summarized here and as detailed in the report.*

Sixteen years after the workshop, the concept discussed therein was realized at least partly by the Tropical Rainfall Measuring Mission (TRMM) in 1997. As soon as the TRMM project was authorized, discussions began with respect to the successor of TRMM. The primary objective of its successor was to expand coverage from low-latitudes to include mid- and high-latitudes, and it was suggested that the essential instruments should be a dual-frequency precipitation radar and a microwave radiometer with additional high frequency channels. Discussion for a TRMM successor then evolved into a constellation system which has a core satellite that provides a standard reference for precipitation measurements, and many other satellites that provide a high sampling frequency (Hou et al. 2014). This concept was eventually realized as the Global Precipitation Measurement (GPM) in 2014. As initially suggested, the GPM core observatory carries a dual frequency precipitation radar (DPR) and a microwave radiometer (GMI).

This review paper briefly presents a history of TRMM as described by Okamoto (2003) and some new findings related to global precipitation measurements. It also describes how techniques used to conduct precipitation measurements from space were developed, presents the GPM concept, and discusses the current situations. This review focuses mainly on radars as these are new global precipitation observation instruments. As the subject area is broad and many important results exist (Houze et al. 2015), the paper is limited largely to Japan’s activities related to TRMM and GPM, and the references acknowledged are far from comprehensive.

2. TRMM

2.1 Objectives of TRMM and precipitation radar

TRMM was originally designed as a “flying rain gauge” (Simpson et al. 1988). It was first conceptualized by NASA in the mid-1980s. Japan collaborated with the program from the onset, and it eventually became a full collaboration between the US and Japan. The planned instruments were a VIS/IR radiometer, a microwave radiometer and a rain radar. At that time spaceborne rain radars had not been realized, although active microwave instruments, such as the synthetic aperture radar (SAR), as well as an altimeter, and scatterometer had been flown in space aboard SEASAT which was operated in 1978 (https://directory.eoportal.org/web/eoportal/satellite-missions/s/seasat).

The final agreement called for the US to provide the satellite bus, the VIS/IR radiometer (VIRS) and the microwave radiometer (TMI), while Japan provided the precipitation radar (PR) and the launch service (Kummerow et al. 1998). The US later added two Earth Observing System (EOS) instruments: the Lightning Imaging Sensor (LIS), and the Clouds and Earth Radiant Energy System (CERES). Both countries were responsible for all planning, data processing, and scientific activities.

The primary scientific objective of TRMM was to obtain precise distribution of rain over tropical and subtropical regions. At that time, the vigorous convections over the tropical western Pacific had already been recognized as the driving engine of the atmospheric general circulation. The Tropical Ocean-Global Atmosphere/Coupled Ocean-Atmosphere Response Experiment (TOGA/COARE) was designed to investigate the interaction between this convection and the tropical ocean (Webster and Lukas 1992). TRMM was originally expected to be ready in time for use in TOGA/COARE which was conducted from November 1992 to February 1993. Unfortunately, the TRMM program was delayed. However, the scientific objective remained, and TRMM was finally launched from the Tanegashima Space Center, Japan, in November 1997.

TRMM was inserted into a 350 km orbit, which was extraordinarily low compared to the heights of other low orbit Earth observing satellites (Table 1). This was necessary because the PR was an active sensor, and its sensitivity was significantly degraded over longer ranges. A second fundamental issue faced by the PR was its narrow swath. Although a wider swath was preferred, technological issues, such as range smearing, broadening of the surface echo at off-nadir angles, and limited dwell time of the radar beam on each pixel prevented wide scan angles. The swath was thus limited to approximately 200 km, and although this was narrow, it enabled individual precipitation systems to be covered.

The designed sensitivity of TRMM PR was approximately 18 dBZ which corresponds to a rain rate of about 0.5 mm h^{-1}. While this sensitivity is worse than ground-based precipitation radars, its real power turned out to be the global observations of precipitation systems regardless of over land or ocean. The disadvantages of rather narrow swath and limited sensitivity to very light precipitation were later mitigated by combining the radar with the microwave radiometers.

Low orbiting Earth observation satellites usually follow sun-synchronous orbits because: (a) the consistent local time observation makes it easy to detect long-term changes in the targets, (b) the small incidence angle change of solar radiation makes the measured data easy to interpret, and (c) the limited sun angle from the satellite reduces the complexity of its thermal design of the satellite. Although the sun synchronous orbit has advantages, TRMM followed a non-sun synchronous orbit. This was mainly because the fixed local time observation causes a bias in the precipitation climatology, particularly in tropical regions where diurnal variations are strong. TRMM’s low inclination orbit of 35 degrees enabled all local time observations to be obtained over one location in approximately 45 days, which meant it could cover the entire diurnal cycle in less than one season. Although an even smaller inclination is better for sampling deep tropical regions, rain associated with the Asian monsoon, which is an important component of the tropical hydrologic cycle, extends to around 35 degree north.

The precipitation radar (PR) was developed by the National Space Development Agency of Japan (NASDA) and the Communications Research Laboratory, Japan (CRL), and it was the technologically advanced instrument. The major specifications of the PR are shown in Table 2. It was a pulse radar with an electrical scanning capability that used a slotted waveguide system to observe precipitation from a satellite moving at about 7 km s^{-1} (Nakamura et al. 1990; Kozu et al. 2001). The PR had a mass of 465 kg and it was the heaviest instrument onboard the TRMM satellite. It used a frequency of 13.8 GHz which was somewhat higher than conventional ground-based rain radars that use 3-10 GHz (S- to X-bands). This frequency selection was a result of many trade-offs. For example, the frequency of 13.8 GHz suffers from rain attenuation in heavy rain; but while a lower frequency would have fewer attenuation problems, it results in a wider radar beam width that degrades the spatial resolution. To provide sufficient spatial resolution, a larger radar antenna was required, which then caused potential of launch vehicle issues. For a downward-looking radar, the radiowave path in rain is typically as short as 5 km which is much shorter than that of a near horizontally scanning ground-based radar, and this mitigates the rain attenuation problem. Another reasons for the choice in frequency was related to the international frequency allocations determined by the International Telecommunication Union (ITU), which arranges frequency allocations to avoid interferences between radiowave services.

To deal with attenuation, a new rain retrieval algorithm, the so-called surface reference technique (SRT) was proposed (Meneghini et al. 1983). This technique uses the surface echo to estimate the total attenuation. Conventional rain retrievals use an empirical relationship between the rain rate (R) and radar reflectivity (Z) called the Z-R relationship (e.g., Battan 1973). The rain-attenuated signal of the PR, however, needed correction before this relationship could be applied. The conventional method used to correct rain attenuation is that of the Histchfeld-Bordan technique (Histchfeld and Bordan 1954). Given a unique relationship between the equivalent radar reflectivity (Ze) and the specific rain attenuation (k), the rain attenuation can be estimated from the measured radar reflectivity (Zm), and the measured radar reflectivity can be corrected to give Ze. When the rain attenuation is weak, this correction by the Histchfeld-Bordan technique works well, but when rain attenuation is strong, the correction becomes unstable. This is because small errors or fluctuations in the measured radar reflectivity or deviation from the assumed k-Ze relationship cause large errors in the attenuation estimate. To overcome the instability, Meneghini (1978) proposed an iterative method to solve the basic equation that relates measured radar reflectivity to the attenuation corrected one. The method allowed only a few iteration, but the problem remained. Because the spaceborne radar looks at the Earth from above, the radar image includes strong surface echoes that suffer from rain attenuation with the amount of attenuation depending on the radiowave path length and the rain intensity. Thus, the reduction of the surface echo from no-rain surface echo constrains the estimated rain intensity. The SRT uses the total attenuation to suppress the instability in Histchfeld-Bordan technique, and this was proven to work well (e.g., Meneghini et al. 2000). The SRT was then successfully incorporated into the TRMM PR rain retrieval algorithms (Iguchi et al. 2000, 2009).

The SRT was not only used for correcting rain attenuation but also for estimating the raindrop size distribution (DSD). Rain retrieval algorithms using radar involves the relationship between radar reflectivity and the rain rate, and this relationship depends on the DSD. Many studies focused on the DSD beginning with the well-known paper of Marshall and Palmer (1948). A known property of the DSD is its dependence on the rain type; stratiform rain contains larger rain drops than convective rain (e.g., Tokay and Short 1996). This concept differs slightly from the intuitive belief that convective rain contains bigger raindrops. This is because convective rain usually has a high rain rate, but the comparison between the DSDs of stratiform and convective rain is made under the same rain rate. Using an estimate of the total attenuation or path integrated attenuation (PIA) of a measured radar reflectivity profile, a correction parameter known as epsilon was derived by the PR and the DPR algorithm development teams. Epsilon is at least partly related to the DSD, and it enables the estimation of DSD variation (Kozu et al. 2009a). Figure 1 shows the global distribution of a proportional coefficient in the power law Z-R relationship derived from the correction parameter and the rain rate. This figure represents the first global distribution of a parameter relating to DSD variation. However, it is of note that the correction parameter does not exactly show the DSD variation because epsilon is affected by many other factors, such as the beam filling effect (Kirstetter et al. 2015), multiple-scattering, attenuation in snow or melting layers, and attenuation due to non-precipitation particles or gases.

The downward looking PR also detects an interesting phenomenon, mirror images of precipitation over the ocean. The ocean surface is a good reflector of microwave radiowaves and the precipitation echo has a mirrored echo that correlates with the direct precipitation echoes. Differences between direct and mirrored echoes are mainly due to sea surface reflectivity and rain attenuation (Meneghini and Atlas 1986; Li and Nakamura 2002). Although such differences have a potential to be used in PR rain retrievals, this has not yet been realized.

The TRMM produced remarkable precipitation images following its successful launch. The first impressive image from the PR was a three-dimensional (3D) image of Cyclone Pam over the Pacific Ocean on 8 Dec. 1997, only 10 days after it had been launched (Hiroshima et al. 1998) (Fig. 2). The image symbolically shows the unique capability of the TRMM PR to observe the 3D structure of a precipitation system over the vast ocean.

The combination of the PR, TMI and LIS demonstrated the full capability for observing precipitation systems. The TMI's advantages over the PR are its wide swath, which is about three times wider than the PR's. The lack of vertical information from the

TMI was overcome using PR's vertical structure of precipitation. This combinational use of data is described in the next section. This has led to better products as well as better sampling not only from TRMM, but also from many additional microwave radiometers onboard other satellites, such as the SSM/I onboard DMSP satellites, and their combined observations have enabled global rain mapping using multi-satellite data. LIS detects lightning which is a good indicator of solid particle existence. LIS and PR data showed that deep convective systems can produce lightning (e.g., Petersen and Rutledge 2001). A global map of lightning yield per rain amount was generated (Takayabu, 2006), and the lightning yield was found to be much higher over land compared to over ocean, which indicates that mixed phase convection is more frequent over land.

In summary, the feature of TRMM is: (a) it followed a non-sun synchronous orbit that enabled diurnal variation of precipitation to be investigated, (b) it had a precipitation radar and microwave and infrared radiometers, which enabled the three dimensional structure of precipitation systems to be investigated, and (c) it worked as a standard reference for precipitation measurements for other spaceborne microwave radiometers, which enabled global rain maps to be developed utilizing satellite data as the primary inputs.

2.2 Long-term observations

It cannot be emphasized enough that the benefits of TRMM were greatly expanded by long-term observations (Houze et al. 2015). The original operation time of TRMM was expected to be only three years. The radar systems were only minimally redundant due to the research nature of the TRMM. Nonetheless, TRMM sensors worked without any serious problems for many years except for CERES, which malfunctioned in the early TRMM operational stages. Ultimately, TRMM's life span was limited by the fuel needed to maintain its orbit. The long term data accumulated resulted not only in the ability to make precise estimation of climatological rain distribution, which was the primary objective, but also in the ability to identify and analyze the evolution of the precipitation systems through the use of composite data from the same season, events, or local time.

Long term observations also provided the ability to observe interannual variability and extreme events; for example, the differences between the precipitation characteristics of El Niño and La Niña. El Niño Southern Oscillation (ENSO) is a well-known teleconnection phenomenon driven by the tropical ocean-atmosphere interaction (Bjerknes 1966, 1969). There, satellite cloud maps was used to show that ENSO is a global scale phenomenon. Precipitation data from TRMM were used to show more clearly that ENSO is a global scale phenomenon. Figure 3 shows the anomalies of precipitation and sea surface temperature (SST) distribution between El Niño and a normal year, which clearly indicate the strong connection between precipitation activity and SST (JAXA 2018). During El Niño, the precipitation maximum moves to the central Pacific, where precipitation has similar characteristics to the deep convection over the western Pacific that occur in normal years (e.g., Berg et al. 2002). TRMM also identified lightning activity in relation to ENSO over Indonesia, and it was determined that activity was stronger (weaker) during El Niño (La Niña) events (Hamid et al. 2001).

The long-term TRMM observations enabled the morphology of global precipitation systems to be identified; not only the distribution of rain but also the structure and evolution of precipitation systems as described later. The TRMM data have also been used widely in investigations of the dynamical structure of the precipitation systems using reanalysis data from ECMWF, NOAA, and JMA.

2.3 Global precipitation maps

The primary objective of TRMM was to obtain rain accumulations over tropical and subtropical regions. Three major types of global rain maps from TRMM have been generated: one from the PR only, one from the microwave radiometer (TMI) only, and one compiled using combinations of PR, TMI, and geostationary satellite data. These have enabled uncertainties in global total rain or zonally averaged rain totals to be considerably reduced (e.g., Kummerow et al. 2000; Adler et al. 2009).

Figure 4 shows an example of annual global precipitation derived from TRMM PR data for 1999-2013 with a 0.1 degree resolution in a Google map style (https://www.rain-clim.com/rainmap.html). The wet regions, such as the intertropical convergence zone (ITCZ), are well depicted. This figure can be compared with that of Dorman and Bourke (1979) (Fig. 5), which was generated from ship data over a period spanning more than 20 years. The progress made using TRMM data is obvious, particularly with respect to spatial resolution. One of the main results of TRMM observations is the ability to identify contrasts between the land and ocean. Although Fig. 4 does not show the coast-line, it is easily identifiable. Prior to the advent of TRMM, it was well known that the maritime continent experiences a significant amount of rainfall; however, the distribution had not been documented. TRMM showed the distribution clearly, and it is evident that large islands receive considerable amounts of rainfall compared to the straits between large islands.

The accuracy of rain maps using microwave radiometer data was greatly improved by using the PR's 3D structure of precipitation systems. Microwave rain retrievals over the ocean are in the so-called emission mode, where strong microwave emissions from rain are clearly detected over weak ocean surface emissions. However, land emissions are comparable to those from rain. Therefore, retrievals of rain over land are made using a scattering mode that uses ice scattering in the upper part of the precipitation system. The amount of ice, or the depth of the solid particle layer, acts as an index that characterizes the precipitation system. However, this retrieval method has an inferior accuracy compared to the emission mode. Microwave radiometers usually have multi-frequency and polarization channels, and rain retrievals use multi-channel data. A well-known retrieval algorithms is GPROF (e.g., Kummerow et al. 2001), which uses typical profiles derived from the PR profiles and computed microwave radiances. The measured data from microwave channels are then used to estimate rain rate via a Bayesian method. The vertical profiles of precipitation systems from PR are essential for this method. The difference between the microwave radiometer derived rain rate and PR estimates was investigated using vertical profiles of precipitation measured by the PR in the early phase of TRMM observations (e.g., Fu and Liu 2001; Berg et al. 2002; Battaglia et al. 2003; Masunaga et al. 2002; Shige et al. 2006, 2008). For example, the discrepancy between PR and TMI rain estimates depends on the depth of the rain layer derived from the height of the bright band observed by the PR (Ikai and Nakamura 2003; Furuzawa and Nakamura 2005).

Compared to the PR, microwave radiometer rain retrieval algorithms developed in the US occasionally produce much lower rain rate over East Asia in summer. Summer rain in East Asia is associated with the Asian Monsoon and is called Baiu in Japan, Meiyu in China or Changma in Korea; the frontal system which produce the summer rain is known as a water vapor front rather than a temperature front (e.g., Ninomiya 1984). The convective instability is not very strong, and both satellite data and ground observations have enabled precipitation to be characterized as driven by warm rain processes. This observation has led to a concept of “wet Asia” where troposphere is humid and the storm top is rather low (Sohn et al. 2010, 2013; Song and Sohn 2015). This fact were strengthened by the results of the precipitation structure during summer monsoon in Asia (Shige and Kummerow 2016; Shige et al. 2017).

There are many other microwave radiometers currently in orbit, and global rain maps, such as TRMM Multisatellite Precipitation Analysis (TMPA) (Huffman et al. 2007; Huffman et al. 2010), GSMaP (e.g., Kubota et al. 2007), and CMORPH (Joyce et al. 2004, 2010), are generated by combining data from a number of microwave radiometers. These maps became successful prototypes for the Committee on Earth Observation Satellites (CEOS) virtual constellation concept (http://ceos.org/ourwork/virtual-constellations/). The virtual constellations are a voluntary based multi-satellite global observation system organized in CEOS, and their themes encompass precipitation, land surface imaging, sea surface temperature, atmospheric composition, ocean color radiometry, and ocean surface topography.

Rain maps initiated using TRMM data are being continuously developed. Large differences are frequently observed between the daily precipitation amount estimated from satellite data and that measured from ground-based instruments. Such discrepancies are due to (a) uncertainty in the rain retrieval algorithm and to (b) poor sampling. Precipitation, particularly torrential rain, has a considerable temporal and spatial variability. To overcome the error source of poor sampling, the idea of the constellation system was proposed in the US in the 1990s. However, even when multi-radiometer data are used, the sampling interval is typically three hours, and short-time torrential rain can be missed. Interpolation techniques are thus applied in global rain mapping, and one example is the motion vector technique. In this respect, geostationary meteorological satellites observe clouds at a high frequency, and the motion vectors of clouds can be derived. The precipitation distribution sampled over a few hours can thus be interpolated using the motion vectors to distribute the precipitation (Joyce et al. 2004; Ushio et al. 2009).

The Japan Aerospace Exploration Agency (JAXA) developed the Global Satellite Mapping of Precipitation (GSMaP) which consists of several rain map versions for various applications. In terms of data latency, near real time data are required for the short-term predictions of weather and flash flood warning. However, climate studies use more accurate data comprised of full auxiliary data, but this requires a longer data latency. The GSMaP currently has several products: a near real time version with four hours latency called GSMaP_NRT, one with a latency of three days (GSMaP_MVK), a gauge-adjusted near real-time version (GSMaP_Gauge_NRT), a non-real time gauge-adjusted version (GSMaP_Gauge), and a real time version (GSMaP_NOW) (Kubota et al. 2020). NASA currently provides a map called Integrated Multi-satellitE Retrievals for GPM (IMERG), which was developed from the TRMM Multi-satellite Precipitation Analysis (TMPA) (Huffman et al. 2020). IMERG has a spatial resolution of 0.1 degree and several temporal resolution versions from 0.5 h to one month (https://gpm.nasa.gov/data-access/downloads/gpm).

The requirements for accuracy of global maps have reached a phase where local precipitation characteristics are incorporated in the rain estimate algorithms (e.g., Aonashi et al. 2009). For example, orographic rain usually has low cloud tops resulting in underestimated rain rate in microwave radiometer retrievals (Kubota et al. 2009). A dynamic selection of lookup tables on the basis of orographic/nonorographic rainfall classification is incorporated in specified mountainous regions (Shige et al. 2013; Taniguchi et al. 2013; Yamamoto et al. 2015, 2017).

Three types of algorithms can be employed to compile rain maps: rain gauge adjustment methods, data assimilation methods, and the use of satellite-based retrieval algorithms. The rain gauge adjustment method (e.g., Mega et al. 2019) is similar to the technique widely used to adjust ground-based rain radar patterns with rain gauge data, such as the radar-AMeDAS composite map provided by JMA (Makihara 1996). This technique is very practical, but the underlying reason for the adjustment is sometimes difficult to comprehend, particularly, in gauge sparce regions. A data assimilation method with atmospheric models is another way. Current atmospheric models are very sophisticated, and most data can be ingested if their accuracy and the error covariance matrices are known. Four dimensional variational (4D-Var) data assimilation or the ensemble Kalman filter method (Kotsuki et al. 2017, 2019; Boukabara et al. 2020; Miyoshi et al. 2020) is a common method used today. Rain maps can be generated as one of the outputs of the models. Here, the rain distribution is dynamically consistent with other atmospheric parameters, such as, temperature and winds. Rain maps can also be produced using satellite data only. In this case, the accuracy of the product depends solely on the capability of the satellite sensors and the rain retrieval algorithms employed. This type of rain maps is independent of the forecast model's assumptions and provide excellent data for use in model evaluations. It should be noted that unlike the gauge adjusted map, the discrepancy between satellite estimates and truth reflects local precipitation characteristics, and such information can be used when conducting studies on local precipitation system characteristics.

The spatiotemporal resolution of global rain maps has been continuously improved, and hourly 0.1-degree resolutions can now be attained. If a climatological map is required instead of an instantaneous map, a satellite rain map can be generated at very high spatial resolution from PR data. As the PR has a pencil beam a horizontal resolution of approximately 4 km at nadir, a very fine rain map can be generated using the long-term accumulation of rain data within finely spaced grid boxes (Hirose and Okada 2018). Precipitation is strongly affected by surface topography which can exhibit large variations. Therefore, climatological precipitation contains fine scale patterns over land relative to the ocean (Hirose et al. 2017; Shige et al. 2017). For example, there are fine scale variations in spatial precipitation over Southeast Asia where large mountain ranges exist, and rain is distributed on the windward side of the mountain slopes (Fig. 6). Remote islands in the ocean may also experience enhanced rain. For example, Yakushima Island covers an area of approximately 400 km^2 and has a mountain with a height of about 2000 m; it experiences 4000 mm of rain annually, and the satellite map clearly shows concentrated precipitation on the southeast side of the island (Fig. 7).

Precipitation measurements from space have an essential role in gaining an understanding of both the global water cycle and the energy cycle. The global energy cycle has attracted considerable scientific attentions with respect to global warming, and the energy transfer between the atmosphere and Earth's surface has been studied in depth. However, there are inherent difficulties in measuring each of the components. The energy input and output to and from the top of the atmosphere are measured by satellites with sufficient accuracy. However, measuring the energy partition in the atmosphere is uncertain. Latent heating is one of the major components of the energy cycle, and energy budget investigations suggested that the observed energy transferred by the release of latent heat is slightly more than that obtained from model estimates (Stephens et al. 2012). As latent heating is closely related to precipitation, it is essential to obtain accurate precipitation measurements to gain a better understanding of the energy cycle. Despite all the advances in radar, radiometer, and composite products, there is still disagreement of perhaps 10% among products.

2.4 Precipitation system climatology

Accumulated rainfall distributions are the most important data used to clarify the global water cycle, and the second most important data are the precipitation system characteristics. For example, even with the same rain total, the type of rain can differ and can, for example, comprise short heavy rain or light persistent rain. In terms of the atmospheric circulation, tall precipitation systems have different effects in the atmosphere than those of widespread light precipitation systems. With respect to societal impacts, torrential rain causes high river discharges, flash floods, and sometimes landslides, while persistent light rain is probably more beneficial. The 3D structure of the precipitation system obtained from the PR opened the era of global precipitation system climatology studies. In this respect, “precipitation system climatology” refers to the precipitation climatology including the storm structures.

Storm top height is one of the indices used to characterize precipitation systems (e.g., Takayabu 2002). The storm height obtained from the TRMM PR is defined as the top of contiguous rain echo bins. For example, Masunaga et al. (2005) used the PR echo-top height and the VIRS brightness temperature to categorize storms. The storm top height also shows large scale characteristics of the precipitation systems. Figure 8 shows the storm top distribution at a latitude of 35 degree north in summer 1998 (JAXA 2018). Very high precipitation systems occur frequently from the Tibetan Plateau to the East China Sea, whereas shallow systems dominate over the eastern Pacific Ocean with cloud tops becoming lower towards the east. Before TRMM observations, the distribution of shallow precipitation over the eastern Pacific was observed by limited ship observations. The TRMM PR showed the distribution of shallow convection for the first time as shown in Fig. 9 (Short and Nakamura 2000). The relationship between deep/shallow convections and the environment conditions was investigated, and it was found that large scale subsidence and SST both control the storm structure over tropical oceans. (e.g., Takayabu 2010).

TRMM data, particularly, PR data can be used to identify areas with deep convection (Zipser et al. 2006; Liu et al. 2007). For example, those within the Congo basin in Africa, the eastern side of the Rocky mountain range in North America, and the deepest precipitations region in Argentina are clearly discernable. While severe rain is generally associated with deep convection, a detailed study showed that deepest convection does not always correspond to the most intense rain for regional extreme rainfall events (Hamada et al. 2015). The relationship between rain rate and the precipitation system structure varies widely, and PR's data on the 3D structure of precipitation system, such as shallow/deep convections and orographic rain, helped better understanding the relationship.

Squall lines in the tropical regions have distinct features; narrow and deep convective lines are followed by widespread persistent (stratiform) rain (Houze 1977). The dynamical structures of convective and stratiform systems differ: convective regions have strong updrafts, while stratiform regions have weak updrafts. Deep convective (stratiform) precipitation indicates a highly (weakly) unstable atmosphere. The DSD characteristics are also different, and these are incorporated into the rain retrieval algorithms (Iguchi et al. 2000; Kozu et al. 2009b). In PR and DPR rain retrieval algorithms, the vertical profile, horizontal extent, and rain rate are used for the precipitation type classification (Awaka et al. 2009; Awaka et al. 2016). In the vertical profile of radar echoes, the melting layer frequently appears as a strong echo layer which is known as a bright band in radar meteorology. The existence of the bright band in measured radar reflectivity is primarily used to identify stratiform rain. The distribution of convective/stratiform rain, the total rain area, the ratio of convective/stratiform types, and rain top heights, are used to identify the precipitation regimes in each season as severe thunderstorms, afternoon showers, shallow systems, extratropical frontal systems, organized systems, and others, as shown in Fig. 10 (Takayabu 2008). The regime characterization of precipitation systems over tropical ocean has also been obtained using a clustering technique and parameters such as the convective surface rain rate, and the ratio of convective rain to total rain (Elsaesser et al. 2010).

It was known that the precipitation systems have different characteristics depending on over land and over oceans. TRMM data updated this view as the characteristics depend on over land, ocean, and coastlines, and suggested a role of the precipitation over coastlines as the dehydrator between the ocean and land (Ogino et al., 2016, 2017).

The monsoon is a tropical phenomenon characterized by significant variations in precipitation, and typically appears in the South Asia and Amazon regions. Precipitation characteristics have been widely studied in the Indian subcontinent region using TRMM data and reanalysis data, and a few results are presented here. In the monsoon season, the Meghalaya region is known for large amounts of total rainfall. TRMM with reanalysis data showed that the peaks of Meghalaya mountain do not extend beyond roughly 2000 m; however, a large amount of humid air is available from the Bay of Bengal, and even a low mountain range triggers large amounts of rain (Fujinami et al. 2017).

It was known from early satellite observations that offshore regions of the Western Ghats in India experience large amount of rain in monsoon season (Krishnamurti et al. 1983; Grossman and Garcia 1990). TRMM observations revealed more detailed distribution of rain around the Western Ghats (Huffman et al. 2001; Adler et al. 2003; Shige et al. 2017). PR identified rainfall maxima on the upslope of the Western Ghats, which neither the GPCP (Adler et al. 2003; Huffman et al. 2001) nor the TMPA (Huffman et al. 2007) did (Shige et al. 2017).

The Himalayan mountain range, the Tibetan Plateau and the northern region of the Deccan Plateau experience large rainfall totals in the monsoon season from June to August with rain that is weak but persistent. In contrast, the total amount of rain in the pre-monsoon season, such as during May, is not particularly high but can have much more intense rain events (e.g., Bhatt and Nakamura 2005, 2006). East-west variations are also evident; precipitation on the west side is more convective than on the east side. Reanalysis data show that the lower atmosphere is very humid over the western region due to wind from the Bay of Bengal, and the upper atmosphere is warm and rather dry in relation to the north wind from the Tibetan Plateau. The atmosphere thus has high convective inhibition (CIN), and rain likely becomes intense once precipitation starts. In contrast, all the troposphere is humid and CIN is low on the east side., which results in persistent but rather weak rain (Houze et al. 2007; Romatshke et al. 2010, Medina et al. 2010).

The seasonal variation in precipitation systems associated with the monsoon has led to the concept of a “green ocean”. Precipitation is generally more convective over land than over the ocean because of strong surface heating and frequent dry air occurring in the middle atmosphere, which leads to strong atmospheric instability. Although it is true that heavy precipitation over land generally occurs during the wet seasons, detailed studies conducted over the Deccan Plateau and Amazon have shown variations in and around the wet season. At the beginning of the wet season, precipitation is associated with strong and high convective systems. In contrast, during the mature wet season, precipitation becomes more stratiform and is associated with slightly lower storm height systems (Petersen and Rutledge 2001; Petersen 2002; Williams et al. 2002). Similar characteristics occur in Bangladesh (e.g., Islam and Uyeda 2008). Lightning activity is strong (weak) in pre- (mature-) monsoon season, which also suggests rather strong (weak) convections in pre- (mature-) monsoon season (Kodama et al. 2005). In other words, the precipitation characteristics over the wet Amazon or Deccan Plateau resemble those over the oceans. The vertical profiles of precipitation over the Deccan Plateau in pre- and mature-monsoon seasons have also been investigated (Hirose and Nakamura 2002, 2004). The precipitation systems are higher for pre-monsoon seasons, and there is a slight reduction in rain content for lower parts of the profiles, which suggests that rain drops evaporate. However, the profile is vertical during the mature monsoon season, which suggests that the entire layer is sufficiently humid.

As previously mentioned, TRMM is in a non-sun synchronous orbit. Since precipitation is strongly affected by solar radiation, it has a distinct diurnal cycle. Over land, this variation is strong, but it is relatively weak over the vast ocean, as there is less thermal forcing from the surface. For example, the land surface temperature easily changes in a range of more than 10 degrees, but the temperature of the ocean surface changes usually in less than 1 degree. The diurnal variation over the ocean occurs in relation to other factors, such as nighttime cloud top radiation cooling or the influence from land such as the land and sea breeze. Long term observations of the TRMM showed that the non-sun synchronous orbit not only avoids the diurnal variation bias in rain totals, but it also helps to investigate the precipitation characteristics with respect to diurnal variations (e.g., Nesbitt and Zipser 2003). Figure 11 shows a map of local time when the rain is at its maximum (Hirose et al. 2008), and it is evident that precipitation over land has an evening or night peak but that over oceans has a morning peak, particularly near the coasts. Figure 12 shows the distribution of isolated precipitation systems at 09:00 and 15:00 local time derived from TRMM PR data, where the different occurrence of the systems at different time of day was evident. Interestingly, the peak local time was found to propagate inland in the eastern part of Brazil or the maritime continent (Fig. 11), and this fact helped to improve the cumulus parameterization of a global atmospheric model (Takayabu and Kimoto 2008). Propagation of the peak local time is also clear over Sumatra and Borneo Islands and the associated dynamical characteristics have been investigated using reanalysis data (e.g., Mori et al. 2004; Ichikawa et al. 2006; Ogino et al. 2016). Such studies have shown that the propagation is characterized by the land and sea breeze embedded in the prevailing monsoon wind. Similar diurnal variations appear over the Tibetan Plateau which contains many lakes, and it has been found that early morning rain likely occurs over large lakes, which suggests that large lakes act like the ocean (Singh and Nakamura, 2009). Over the Western Ghats and Myanmar coast, large rainfall amounts with small amplitude of diurnal variations are observed under strong environmental flow implying that rainfall is associated with mechanically driven convection (Shige et al. 2017).

The diurnal characteristics of precipitation provide evidence of the difference between the pre- and mature-monsoon or the active/break monsoon similar to the green ocean concept. The diurnal variation of precipitation is stronger during the pre-monsoon season than the mature monsoon season, which indicates an existence of an unstable atmosphere (Bhatt and Nakamura 2005). Similarly, the diurnal variation is strong (weak) over the Deccan Plateau in the break (active) spells of the monsoon (Singh and Nakamura 2010). Furthermore, the amplitude of the diurnal cycle over the upslope of the Western Ghats is smallest in the intraseasonal oscillation rainfall anomaly phase during the largest boreal summer, and it is largest during the large scale active phase (Shige et al. 2017). Another example comes from mountainous regions; distinct morning rain occurs over the southern slope of the Himalayas, and the near surface wind shows significant diurnal variation and becomes mountain (valley) wind in early morning (evening). In accordance with the wind variation, precipitation also shows diurnal variations with notable morning rain peaks associated with the convergence between prevailing monsoon wind and the morning downwind over the slope (Fig. 13) (Bhatt and Nakamura 2006).

A typhoon is a typical large scale atmospheric phenomenon generated over regions of warm water, such as the tropical western Pacific. Their accurate and timely forecasts are crucial for disaster prevention. TRMM observations of typhoon over vast ocean areas increased the understanding of the structure of typhoons (e.g., Cecil and Zipser 1999; Hoshino and Nakazawa 2007; Yokoyama and Takayabu 2008).

2.5 Evolution of precipitation systems

TRMM observation data represent accumulated snapshots. The time evolution of precipitation systems is not directly observed, but long-term observations can be used to collect statistics of the evolution of precipitation systems. One example is the diurnal variations in scales of the precipitation system; many small systems firstly appear and these systems aggregate and evolve to large and vigorous systems (Hirose and Nakamura 2005). Long-term TRMM observation data can also be combined with data from geostationary meteorological satellites, which observe cloud distribution continuously using the VIS/IR technique. Combining various local time observations with the continuous geostationary satellite data can at least partly overcome the difficulties involved in studying the evolution of precipitation systems. Geostationary satellite data show the extent of clouds and their top heights, and the PR and TMI observe the structure of the precipitation system. Using the TMI, PR and geostationary satellite data, the evolution of a precipitation system over the tropical Pacific Ocean was investigated, and the results showed that the systems were initially small and low prior to evolving into a deep strong system with intense rain, finally became wide systems containing a large amount of stratiform rain and expanded high clouds (Kondo et al. 2006; Imaoka and Nakamura 2012). This evolution process is also reflected in the peak local time differences of brightness temperatures observed with VIRS and TMI, and of the surface rain rate observed with PR (Yamamoto et al. 2008). This type of evolution has been observed in a limited number of field experiments, and the long-term observation data of TRMM validate these characteristics statistically.

Composite analyses have been widely conducted using TRMM precipitation data along with other satellite data, such as OLR or reanalysis data. A popular method used to obtain the characteristics of the system of interest is to conduct an analysis with composite maps, the center of which (e.g. an area of intense precipitation) moves with the system. Equatorial regions have distinct intraseasonal variation, such as the Madden-Julian

Oscillation (MJO) (Madden and Julian 1971, 1972), and the characteristics of the MJO have been investigated with respect to the equatorial Rossby wave and Kelvin wave (Masunaga et al. 2006). A relationship between El Niño and MJO was also shown by Takayabu et al. (1999). Composite analyses using TRMM and A-train satellites revealed interactions between large scale disturbances and the precipitation systems including convective mass flux (Masunaga 2012, 2013; Masunaga and Luo 2016). A moisture budget has also been analyzed to show the structure of equatorial inertia-gravity waves (Sumi and Masunaga 2016). Another example is the relationship between precipitation characteristics in the Baiu front and the subtropical jet using TRMM PR, and reanalysis data (Yokoyama et al. 2014, 2017). These examples indicate that TRMM data have become a standard and essential dataset used to study the relationship between large scale atmospheric conditions and precipitation characteristics.

2.6 Latent heating

Latent heating is not only an important component in the global energy balance but also one of the major drivers of the general circulation. The column total latent heating is equivalent to the surface rain when a sufficiently large area is considered, and the total column latent heating can be determined when an accurate distribution of the rain is obtained. However, the vertical profile of latent heating is essential to understand the driving mechanism behind the general circulation. In ground observations, the vertical profile of latent heating is generally obtained from heat and moisture budgets along with wind data. Wind data are generally not obtained from satellites, with the exception of wind vectors derived from cloud images of geostationary satellites or the sea surface wind derived from scatterometers. However, as the wind vectors derived from geostationary satellites had coarse vertical resolution, the global 3D structure of latent heat release was not available. TRMM observations discriminate precipitation systems into convective and stratiform systems. Field experiments, such as the GARP Atlantic Experiment (GATE) in 1974 (Kuettner 1974) or TOGA/COARE have shown that heating profiles differ depending on the convective/stratiform rain types (Mapes and Houze 1995; Houze 1997). It has been determined that convective precipitation causes heating in all levels, whereas stratiform precipitation causes heating in the upper levels and cooling in the lower levels due to evaporation (Fig. 14). Heating profiles of convective and stratiform precipitation systems were derived based on the results of field experiments in addition to fine scale non-hydrostatic model results. Global latent heating profiles were then obtained using TRMM's convective/stratiform rain classifications (see a reviews by Tao et al. 2006, 2016). A few major algorithms for latent heating are currently available. One of them was developed at the Goddard Space Flight Center, NASA, and it originally used TMI and PR data that provided information about convective/stratiform classifications and the surface rain rate, and latent heating is obtained in the wide swath of microwave radiometers (Takayabu and Tao 2020). Another algorithm is developed in Japan, and it uses PR precipitation profiles

(Shige et al. 2004, 2007, 2008, 2009). The rain types, rain rate at the surface, rain rate at the height of the melting layer, and the storm top height are used as the input parameters for model latent heating profiles, but retrieval is limited to the PR swath. The algorithm produces a reasonable 3D latent heating structure (e.g., Fig. 15). Both algorithms use lookup tables generated from cloud resolving models, and they provide not only the latent heating (apparent heat source) but also the apparent moisture sink.

2.7 Validation

Remote sensing is used to observe the Earth environment from satellites. However, it is rare that the required physical quantity, such as surface rain rate in the case of TRMM, can be measured directly by the instruments onboard satellites, and retrieval algorithms are thus used. Many assumptions are made in this respect, which cause discrepancies between estimates and the truth. Validation of estimates and the development of retrieval algorithms are being continually conducted.

Many countries, such as Japan, the US, and Korea have dense rain gauge networks, and the most conventional method used to make precipitation measurements reliable is to compare satellite surface rain estimates with ground-based rain measurements. Both instantaneous and accumulation comparisons were made. Instantaneous comparisons were made between ground-based radar images and satellite images, and to mitigate the spatial and temporal differences between the observations, spatiotemporal interpolation was usually applied. The resulting similarity between the rain distributions obtained was remarkable, and the results confirmed the validity of mapping rain distribution from spaceborne instruments. With respect to the PR, comparisons between PR reflectivity and that from the ground-based radar were conducted, which was a more direct comparison than using rain rates. The correlation between radar reflectivities was usually good, but biases have been found between the results. Discrepancy have mainly been attributed to ground-based radar calibration errors rather than those of the PR. The original idea behind making comparisons was to validate satellite-measured radar reflectivity, but what was quickly found is that ground-based radar can be calibrated by TRMM PR (Anagnostou et al. 2001; Warren et al. 2018).

With respect to comparisons of accumulated rain, many investigations have been conducted in various countries using rain gauge data. Such investigations are essential for enabling the real application of satellite rain maps in, for example, the water resources management and flood forecasts in these countries. Satellite rain maps generally provide good data when using seasonal accumulation, whereas rain totals over short time scales, such as, daily rain totals do not always show good results. The precipitation maps using primarily satellite data are internationally validated using ground observations as the activity of the International Precipitation Working Group (IPWG) established as a permanent Working Group of the Coordination Group for Meteorological Satellites (CGMS) (Kidd et al. 2020b).

Rain retrieval algorithms invariably use assumptions. To validate these assumptions and evaluate the estimates, several specific field experiments have been conducted. For example, an aircraft experiment was conducted by NASA to validate SRT (Durden et al. 2003). In this experiment, variation in ocean surface radar signatures were measured, and the result provided uncertainty estimates for SRT. In addition to specific experiments, NASA also conducted several comprehensive field experiments using both ground-based and aircraft observations. The aircraft observations were conducted to provide in-situ data of cloud and precipitation particles as well as to simulate satellite observations. One example was the TRMM-Large Scale Biosphere-Atmosphere Experiment in Amazonia (TRMM-LBA), which was conducted over the Amazonian regions from 1 November 1998 to 28 February 1999 (https://cloud1.arc.nasa.gov/trmmlba/overview.html), in which the precipitation characteristics associated with the South American monsoon were investigated (e.g., Petersen et al. 2002). NASA also conducted a field experiment around Kwajalein Atoll (KWAJEX) in the tropical Pacific in 1999 (e.g., Houze et al. 2004), and many results relating to convection over the tropical ocean were accumulated. Many of these studies included direct comparison of PR data with ground-based radar data (e.g., Schumacher and Houze 2000). NASA has continued to conduct large field experiments such as the Mid-latitude Continental Convective Clouds Experiment (MC3E) in 2011, and the Olympic Mountain Experiment (OLYMPEX) in 2015-2016. OLYMPEX was conducted to observe snow in mountainous regions in relation to GPM. In Japan, a small field experiment, the Ishigaki/Miyako Campaign Experiment for TRMM (IMCET), which included observations by ground-based and airborne radars, was conducted to validate TRMM PR rain observations (Hanado et al. 1998).

According to the results of statistical comparisons of ground-based observations and estimated rain totals, discrepancies between estimates and truth were investigated. For example, missing rain due to the limited sensitivity of PR causes underestimates (Shimizu et al. 2009). Another example is the extrapolation of vertical profiles of precipitation echo to the surface. The PR cannot always detect rain near the surface. This phenomenon particularly occurs near the edge of the radar scan, where surface echo contamination expands, and surface rain is estimated from the rain in contamination free layers. This extrapolated estimate is called “e_SurfRain” in the PR products. However, when the rain profile deviates from being uniform, extrapolation will have errors (Hirose et al. 2012).

3 GPM

3.1 Objectives of GPM

After the remarkable success of TRMM, scientists aimed to expand the coverage over the limited tropical and subtropical observations of TRMM. To accomplish this, the GPM was designed. Solid precipitation frequently falls in high latitude regions; therefore, accurate water-equivalent snow fall estimates are necessary to provide the precipitation total in high latitude regions. To obtain these, the use of a dual-frequency radar was proposed, and ultimately realized as the DPR (Okamoto 2003). It is of note that the original design of the TRMM PR was a dual-wavelength radar, but it was descoped to a single frequency radar due to budget limitation. The DPR employs 13.6 and 35.5 GHz radiowaves which are very similar to the originally proposed PR frequencies of 13.8 and 35 GHz (Table2). The radar type is also the same as the planar slotted waveguide active array system with two-frequency agility. The development of the DPR, however, was simpler than the original PR with respect to some component such as the phase shifter, owing to the development of microwave technology. Following the successful launch, it was found that the sidelobe clutters in 13.6 GHz radar (KuPR) data were stronger than expected, but the clutter was sufficiently suppressed after tuning the phase shifters (Kubota et al. 2016).

The core observatory of GPM is equipped with the DPR and a GPM microwave radiometer (GMI) and its inclination angle is 65 degrees which is much higher than that of TRMM (Table 1). The GMI is more advanced than the TMI, and it adopts additional new high frequency (166 GHz and 183 GHz) channels, which are the water vapor channels required to detect snowfall. The GMI has a much larger antenna of 1.2 m than the TMI, which results in a better spatial resolution (Hou et al. 2014; Skofronick-Jackson et al. 2017).

3.2 DPR performance

The DPR was included in the GPM to observe 3D structure of precipitation systems over regions where TRMM PR did not cover. For example, vertical structures were compared between tropics and extratropics (Kobayashi et al. 2018), and downward increasing profiles of rain due to warm rain process were identified. The characteristics of precipitation over Alaska were investigated by Aoki and Shige (2021). Coastline and mountain effects appear clearly in their analysis (Fig. 16).

The DPR also enabled the following: (a) observations of weaker precipitation systems, (b) better liquid/solid precipitation discrimination, and (c) more accurate rain rate retrievals. The sensitivity of the DPR’s Ku-radar (KuPR) is a few dB higher than the originally designed value, thanks to the increase in transmitted power and improvements made to the receivers. The sensitivity of the DPR’s Ka-radar (KaPR) was the same as its design (Kojima et al. 2012; Masaki et al. 2020). The sensitivity was also investigated using statistics of KuPR and KaPR reflectivities (e.g., Toyoshima et al. 2015; Hamada and Takayabu 2016). Thus, the objective (a) was attained by both KuPR improvement and the inclusion of KaPR. The second objective (b) has been attained as, for example, a new heavy ice flag was added to the DPR dataset (Iguchi et al. 2018). Large ice particles can result in a strong Mie effect, which deviates scattering from simple Rayleigh one. Using the heavy ice flag, a heavy ice precipitation band was detected in an extratropical cyclone (Akiyama et al. 2019). Furthermore, in the bright band or the melting layer, precipitating particles are large, and a significant Mie effect occurs, which results in a difference between KuPR and KaPR radar echoes: therefore, another application was designed to improve bright band detection (Le and Chandrasekar 2013a, 2013b). The convective/stratiform rain type classification was improved by using the improved bright band detection algorithm (Awaka et al. 2016). The third objective (c) to provide accurate rain rate retrievals, is challenging, but progress has been made (Seto and Iguchi 2011, 2015; Seto et al. 2013, 2021). Conceptually, additional information in the difference between two profiles of Ka- and Ku-band radiowaves can contribute to improvements in rain retrieval. As the two beams of the radars are designed to match each other, the difference occurs in relation to the frequency dependence of the scattering cross sections of the precipitation particles and attenuation within the radio path. This frequency difference appears as the Mie effect in the Ka-band, and the difference depends on the DSD. Attenuation is mainly due to rain particles at the Ka-band. If the Mie effect is ignored, the rain rate can be estimated from the attenuation. The idea of obtaining rain rate estimates from rain attenuation began in the 1970s for a ground-based radio path (Atlas and Ulbrich 1977). A modified method for a spaceborne radar using both Ka and Ku-band rain profiles was proposed by Kozu and Nakamura (1991). However, several obstacles remain: as the two profiles are similar, the resulting rain rate is sensitive to small differences of the two reflectivity profiles which occur due to the beam filling effect, the multi-scattering effect, attenuation from non-precipitating materials, or deviation of the

DSD from assumed one. When precipitation is not uniformly distributed in radar pixels, the simple dual-frequency technique contains biases (Nakamura 1991). Multiple-scattering is another problem. This is evident in data obtained from the spaceborne W-band (94 GHz) cloud profiling radar (CPR) onboard CLOUDSAT (Battaglia and Simmer 2008), and is significant even in Ka-band radar images of heavy rain (Battaglia et al. 2015). SRT has been improved using DPR surface signatures, as surface signatures in the Ku-band and Ka-band have good correlations, and PIA estimations have been improved (Meneghini et al. 2012, 2015, 2021). The global distribution of DSD became more precise using DPR data as shown in Fig. 17. The coverage of the distribution of DSD was also extended to midlatitude regions. The mass-weighted mean diameter and the precipitation rate show different distributions, and it has been shown that estimated DSD variations related to the structure of precipitation system (Yamaji et al. 2020). The DSD variations at least partly explain the difference between PR-estimated rain rate and TMI estimated rain rate. In addition, the DSD variations have been incorporated in the DPR rain retrieval algorithm (Seto et al. 2021).

The KaPR has two scan modes: one is the matched scan and the other is high sensitivity scan. The pixels of the matched KaPR scan were matched with those of the KuPR, and in the original scans of the DPR, high sensitivity pixels were interlaced in the matched scan. After evaluating the sensitivity of radars, the high sensitivity mode scan was moved to the outer band of the normal scan of KuPR in May 2018, which resulted in extension of the KaPR swath. Therefore, the swath in which dual frequency data are available has been expanded (Iguchi 2020).

The DPR uses the first ever spaceborne Ka-band (35 GHz) precipitation radar. However, the radiowave scattering characteristics of precipitation particles are complex compared to those of other lower frequency radiowaves. This difficulty is exacerbated for snow observations, particularly, when observing melting snow, as shapes, densities, and water mixing ratios vary widely (e.g., Liao et al. 2021). Although many model calculations have been conducted to provide radiowave scattering characteristics of snow particles or melting snow particles, uncertainty remains. Ground observations is another method to investigate the scattering characteristics, and JAXA developed a dual Ka-band radar system consisting of identically designed Ka-band radars to assist in this approach. By positioning the radars to face each other, the precipitation system between the two radars can be observed simultaneously by both radars. As rain attenuation is significant in the Ka-band, and radar signature weakens over longer ranges, equivalent radar reflectivity and specific attenuation can be directly measured. Different scattering characteristics of dry/wet snow and rain were obtained (Nishikawa et al. 2015; Nakamura et al. 2018).

3.3 Transition from PR to DPR

TRMM’s PR was the first spaceborne radar, and its operational period was extended from the original three years to 17 years. Thanks to this long observational period, climatological studies have been significantly advanced. The GPM DPR is a new version of this spaceborne radar, and the studies of precipitation trends in the climate change era are continuing. However, to avoid the misidentification of climatological trends, well calibrated data are required. Many spaceborne Earth observation instruments, such as microwave radiometers, have technological experiences to continue data without gaps or jumps over multiple spaceborne radiometers, whereas, for spaceborne precipitation radars, the only transition has been from the PR to DPR. The PR itself had experienced problems with data continuity. In 2001, TRMM's orbit was boosted from a height of 350 km to 400 km in order to extend its lifetime. The PR's sensitivity and spatial resolution were altered because of the change of the satellite altitude, and a small mismatch between the transmitting pulse and the received radar echo also occurred. Nevertheless, almost all of the deviations were recognized and understood in the statistics of rain totals and storm height (Shimizu et al. 2009; Hirose et al. 2012; Kanemaru et al. 2019). Another incident occurred in 2008 when a part of the PR malfunctioned, and the part was switched to redundant one. Slight variations in the system parameters, such as noise levels, occurred. System calibration was conducted using internal house-keeping data and a ground-based external active calibrator that transmitted or received radiowaves to and from the PR (Kanemaru et al. 2017; Masaki et al. 2020). The accuracy of data continuity was subsequently evaluated and confirmed using the statistics of rain totals, storm top height, and long-term rain total trends.

Engineering calibration of the PR or DPR is performed to ensure that it fluctuates by less than 1 dB in operation periods (Takahashi et al. 2003; Shimizu et al. 2009). This long-term calibration stability is remarkable and illustrates a considerable engineering success. However, the accuracy is not yet sufficient for use in detecting climate change. Fluctuations of 1 dB in radar reflectivity correspond to a rain rate of approximately 15 %. Therefore, another calibration is necessary. TRMM and GPM use radar signatures of the sea surface with no rain to obtain precise radar beam widths and pulse widths (Kanemaru et al. 2020).

Special operations of the PR were performed from October 2014 to January 2015 near the end of TRMM's life-time, which was determined by the amount of fuel remaining (Takahashi et al. 2016; Takahashi 2017). During normal observations, the PR beam scanned cross-track directions, and the scan angles were limited. Near the end of the mission, the altitude of the satellite decreased, and the normal operational data were not available. In this period, wide scan operations, dense observations, and a 90 degree yaw maneuver were performed. The wide scan operation was conducted to investigate surface clutter interference. When the radar beam had a large incidence angle, surface clutter contamination is significant, and this is one of the factors preventing observations at large incidence angles. The result showed that although surface clutter was broadened and contaminated the precipitation echo at incidence angles far from nadir, the intensity of the surface echo was reduced. The result suggested that the use of a wide-angle scan may be possible when moderate to heavy rain is being measured (Yamamoto et al. 2020). During dense observations, the beam scanned only near nadir angles, and one location on the Earth's surface was observed with fine spacing over-sampled data. In the normal scan of the PR, the pixels were separated with the radar beam width, but a better spatial resolution could be obtained from oversampled data. The 90 degree yaw maneuver operation showed a better relationship between surface signatures and incidence angles. In the normal cross track scan, different surfaces were observed with different incidence angles, but in the 90 degree yaw maneuver, the scan became along-track, and fixed point signatures with different incidence angles were obtained in about 30 seconds. This provided data for studying SRT uncertainty.

3.4 Applications

Many applications using precipitation data from satellites, which were in the test and validation phase during the TRMM era, have become operational in the GPM era. Water vapor or precipitable water obtained from microwave radiometers, particularly, over oceans is important for weather forecasts, and these data had been assimilated in numerical models. While water vapor data from microwave radiometers predated TRMM was used, data from TRMM TMI and later GPM GMI have been added to the assimilation suite. However, it is difficult to assimilate precipitation, because the distribution of precipitation has fine spatial variation and spatial mismatches with the model likely cause errors. Therefore, a spatial matching method has been developed (Aonashi et al. 2011), and the technique is currently operationally applied. Studies have also attempted to assimilate the vertical profile of precipitation from DPR (Aonashi et al. 2014; Okamoto et al. 2016, Ikuta 2016; Ikuta et al. 2020).

The development of atmospheric models has been remarkable partly thanks to the enormous expansion in computer power, such as the Earth Simulator of the Japan Agency for Marine-Earth Science and Technology (JAMSTEC). At the start of the TRMM era, the spatial resolution of global atmospheric models was typically 100 km, but the spatial resolution of satellite observations was typically a few tens of km. Today, the global model resolution is superior to that of satellite observations (e.g., Satoh et al. 2014). The model is non-hydrostatic and does not use cumulus parameterization, therefore, the model results can be directly compared with satellite observations, which greatly assists in the validation or evaluation of model results (e.g., Kotsuki et al. 2014).

The improvements made in compiling global precipitation maps enable the maps to be used in flood forecast, and in this respect, the Integrated Flood Analysis System (IFAS) was developed in the International Centre for Water Hazard and Risk Management, Japan (ICHARM) (http://www.icharm.pwri.go.jp/research/ifas/) (Tsuda et al. 2014; Kidd et al. 2020a). This system uses global precipitation from GSMaP as the primary input data and forecasts river discharge using hydrological models. The alert maps and information are available on the websites of the Global Flood Alert System (GFAS) or the International

Flood Network (IFNET). A parallel system, the Global Flood Monitoring System (GFMS) developed in the US, uses IMERG data as the input data (Wu et al. 2014). Global precipitation maps are also used to detect extremes and droughts based on long-term observation data (e.g., Kuleshov et al. 2020; Tashima et al. 2020).

With improvements in the reliability of the satellite rain maps, associated applications have greatly expanded. One example is an application for dengue fever outbreaks. Mosquitoes are vectors of dengue fever, and their populations depend on water. Precipitation data can thus be used to investigate the relationship between precipitation and dengue fever outbreaks (e.g., Igarashi et al, 2014; Pham et al. 2018). The relationship between cholera outbreak and precipitation was also studied (JAXA 2019).

The global rain distribution is also used to monitor global crop harvest. Although the growth of the crops is mainly monitored by infrared radiometers, crop yields depend on rain, and precipitation is thus one of the important data to enable accurate crop yield prediction to be made (Oyoshi et al. 2016; Kidd et al. 2020a). In addition, hydropower is an important energy source in mountainous countries, and when the regions are poorly precipitation-gauged, global precipitation maps can be used to make assessments of suitable hydropower locations (Mori et al. 2020). Furthermore, the global precipitation maps can be used for the weather derivative in insurance applications (JAXA 2019). As such, global precipitation maps are now part of the international infrastructure.

4. Beyond GPM

As the TRMM successor discussions were initiated once TRMM's success was apparent, discussions about new precipitation measurements after GPM have already begun (Battaglia 2020). Long-term climate records are essential for conducting climate studies, and the importance of data continuity is strongly emphasized during all Earth observation satellite discussions. Technological developments are continually made, and new instruments have improved capabilities that provide new data and enable new findings. Thus, a new Earth observation satellite must provide (a) continuity of the physical data from instruments that include the capability of the previous instruments, and (b) data from new instruments. The emphasis ultimately depends on the funding agencies. JMA or NOAA, being operational agencies, they may emphasize (a), while NASA and JAXA are research and development agencies and they may emphasize (b).

Although global precipitation observations are being continuously improved, there is still a long way to go. Some targets for future developments are described as follows.

(a) To provide precise rain totals needed for detecting changes in the global rain accumulations occurring within the context of global climate change

The global rain total over land has increased by nearly 1 % in the last 100 years. According to the Clausius-Clapeyron (C-C) law, an increase of 1 K corresponds to a few percent increase in saturated water vapor pressure. In this respect, precipitable water has shown an increasing trend consistent with surface temperature increases, particularly over the ocean (IPCC 2013). Therefore, if the cycling speed or resident time of water vapor in the atmosphere does not change, the amount of total precipitation would increase by a few percent. However, despite surface temperature increase, GPCP data from post-1979 show only a weak increasing trend in global total rain. It has increased in tropical regions, but the increase has been offset by decrease in extratropical regions. (Gu et al. 2007; Adler et al. 2008). For better understandings of the trend of the global rain totals, precise rain total data are required (e.g., De Meyer and Roca 2021).

(b) To provide higher temporal and spatial resolution precipitation maps

In the era of rapid atmospheric model improvements, spatiotemporal resolutions of the observations from space must be at least compatible with those of models to enable the model result to be evaluated or validated. Higher resolution is also required to provide precise rain total estimates for local precipitation characteristics. For real applications, such as short-range flood forecasts, current spatial and temporal resolutions are too poor. An example is river discharge prediction. Precipitation over land is strongly affected by topography, and precipitation over one side of a mountain ridge has big impacts on river discharge relative to when precipitation occurs over the other side of the ridge.

(c) To attain precise measurements of water equivalent solid precipitation

High latitude regions experience solid precipitation. To close the water budget of the global water cycle, water equivalent solid precipitation measurements are required, even though there are low total amounts of precipitation at high latitudes. For the snow measurements from space, the microwave signature of snow is weak, and backscattering cross sections are small. In addition, snow particles, particularly, melting snow particles have a wide range in size, and their permittivity differs due to the mixing ratios of ice, water and air. Therefore, snowfall measurements remain a challenge. Even on the ground, snowfall measurements have large uncertainty related to variation in the gauge catchment ratio due to wind or the mixing of ground snow blown by wind. This fact gives another problem for validation of the snowfall measurements from space.

Currently there are two major pathways for defining the objectives of a potential DPR successor. The first one is to understand the interactions between aerosols, clouds, and precipitation. Aerosols act as the nuclei of water vapor condensation and produce cloud particles, and the capability of aerosols to produce cloud particles depends on their size, chemical properties, and the water vapor saturation ratio and temperature. For example, generally, high number densities of aerosols result in a large number of small cloud particles that suppress precipitation (Rosenfeld 1999). This mission pathway includes an aim to understand the conversion mechanism from clouds to rain. It also addresses the effect of cloud properties on the radiation budget to enable accurate climate change modelling. The original mission concept was proposed in the US decadal survey for Earth Science and Applications from Space (National Academies of Sciences, Engineering, and Medicine 2019) and it evolved to the more comprehensive Aerosol, Cloud, Convection and Precipitation Study (ACCP). The other major pathway aims to gain a better understanding of the global water cycle. Precipitation is a crucial component, and accurate and precise measurements of precipitation are required. Although data from TRMM and GPM and combinations of other data have dramatically improved the ability to obtain global precipitation amounts, uncertainty still remains. To improve the accuracy, global coverage that includes high latitude regions, and accurate water equivalent snow measurements are required. Currently one of the biggest obstacles for improving the accuracy of rain totals is the sampling frequency of satellite observations. To overcome this obstacle, a core observatory with constellation satellites as with GPM, is necessary. This core observatory should be equipped with an advanced precipitation radar in the Ku-band that has better sensitivity and a wider swath than the DPR. Current advanced precipitation radar studies have suggested that better sensitivity can be attained using final stage high power amplifiers, and a larger antenna than current PR or DPR (Kummerow et al. 2020). The larger antenna enables Doppler measurements to be conducted. The Doppler function is a promising new capability to measure vertical velocity of precipitation particles at nadir. Obtaining the vertical velocity would assist in precipitation particle discrimination and in the characterization of dynamical structures of precipitation systems. It would also contribute to improving the latent heating estimation, as heating is correlated with the vertical air motion.

The importance of spaceborne precipitation radars is well recognized, but other technologies perhaps need to be developed, rather than continually upgrading current technology. This could be achieved using small satellites. The development of big satellites is extremely expensive and time consuming for development, and observations using a large number of small satellites could mitigate the low sampling frequency problem (e.g., Yamaji et al. 2019). One example is that of the US RainCube (Peral et al. 2019), which is a Ka-band fixed beam radar system onboard a small satellite that was released from the International Space Station (ISS) in 2018. RainCube is a 35 GHz radar with a 0.5 m antenna. It demonstrated the technological feasibility of using a small low cost satellite. However, the performance of the instrument onboard the small satellite is limited, and a reference standard such as the GPM core observatory may still be needed. Another challenging idea is to use a large radar in a geostationary orbit (Im et al. 2004). This concept was initiated in 1980s (Gogineni and Moore 1989). Precipitation could be observed almost continuously from the geostationary orbit in a similar manner to the geostationary meteorological satellites, thus solving the sampling problem. To obtain sufficient spatial resolution, a Ku-band active array radar system using an antenna measuring 30 m by 30m is currently studied in JAXA (Okazaki et al. 2019).

5. Conclusions

TRMM was launched in 1997 and provided the global distribution of rain with significantly improved accuracy. TRMM paved the way for two types of studies: global precipitation system climatology, and precipitation measurement technology from space. Prior to the advent of TRMM, precipitation science had focused on the occurrence and distribution of precipitation using ground observations that includes the use of 3D structures from radars. The ground observations enabled the identification of many types of precipitation systems, such as tall convection, wide extended stratiform, shallow orographic, and large precipitation associated with frontal activities. Previous studies had also focused on the internal structure of 3D precipitating particle distribution, and the corresponding air motions in different precipitation types. However, almost all observations were limited to local scales, and global precipitation observations were mainly limited to the distribution of rain on the ground. Global 3D structure observations of TRMM overcame these limitations at least partly, even though coverage was limited in tropical and subtropical regions.

GPM is the formal successor of TRMM. GPM has expanded coverage to +/- 65 degrees in latitude and includes measurements of solid precipitation. The GPM core observatory has been providing data for more than six years since its launch in 2014, and is currently healthy. Along with the 17-year data of TRMM, precipitation data obtained from space are essential for studying climate change. Studies of precipitation system climatology can now be extended to high latitudes. Over tropical regions, the Coriolis parameter is small and the divergence/convergence of the flow are of primary importance in the atmospheric dynamics. In contrast, from mid to high latitude regions, the Coriolis parameter is large, and vorticities are of primary importance. This fact characterizes the dynamical structure of tropical and extratropical atmosphere (e.g., Satoh et al. 2008; Matsuno 2017). It is said that tropical regions are the Velocity Potential (VP) World, while the extratropical regions are Potential Vorticity (PV) World. In the VP world, latent heat release associated with precipitation is the major driving force of atmospheric disturbances, whereas in the PV world, baroclinicity is the major cause of disturbances, and precipitation is generally a consequence of disturbances. In tropical regions, typical precipitation systems are squall lines, vigorous tall convections, super clusters, and tropical depressions. In extratropical regions, precipitation associated with extratropical depressions and frontal systems is much more important, while that associated with polar lows and shallow convections induced by cold air outbreaks also frequently occur. Thus, types of precipitation systems can be more widely identified and refined using GPM data.

Based on the remarkable progress of atmospheric models, satellite data can be merged or assimilated in global numerical models, and comprehensive datasets can be generated. Datasets naturally include precipitation information, and data are consistent under model assumptions; therefore, reasonably good datasets are currently provided about Earth’s atmospheric environment. There is still a demand for datasets that are independent of model outputs, and observations with higher accuracy and better spatiotemporal resolutions are still required.

Rapid progress in the increase of computer power has opened new avenues with respect to the use of artificial intelligent technology (AI), such as deep learning, neural networks, and random forest. AI has been widely tested for use with retrieval algorithms of Earth observations from space, particularly in land cover identifications, and has also been applied in global precipitation mapping (e.g., Sorooshian et al. 2000; Nguyen et al. 2018; Hirose et al. 2019). Athough AI has a potential, however, it has limitations in that the results are sometimes difficult to interpret.

Several books on precipitation measurements from space have been published to date. For example, “Tropical Rainfall Measurements” (Theon and Fugono 1988) was published in 1988, prior to the launch of TRMM, “Measuring Precipitation from Space” (Levizzani et al. 2007) was published in 2007 while TRMM was in orbit, and recently, “Precipitation Measurement from Space” (Levizzani et al. 2020a, 2020b) has been published. These books represent the remarkable progress of the precipitation measurements from space.

Acknowledgments

TRMM and GPM projects were made possible by the work of many engineers and scientists, but it is impossible to list and thank all collaborators. The author would therefore like to thank and acknowledge the institutes that deeply involved in the projects: JAXA, NASA Goddard Space Flight Center, the National Institute of Information and Communications Technology (NICT), Colorado State University, Nagoya University, and the University of Tokyo. The author would also like to express deep gratitude to the founders of TRMM and GPM who are no longer with us: J. Simpson, D. Atlas, Tsu. Nitta, O. Thiele, A. Hou, and T. Kozu. The author is much grateful for anonymous reviewers and the editor of the Special Issue who gave me many invaluable comments including many appropriate references. This work is partly supported by JAXA Precipitation Measuring Mission (PMM) project.

References

Adler, R. F., and Coauthors, 2003: The version-2 Global Precipitation Climatology Project (GPCP) Monthly Precipitation Analysis (1979–present). *J. Hydrometeor.*, **4**, 1147–1167, doi:10.1175/1525-7541(2003)004,1147:TVGPCP.2.0.CO;2.

Adler, R. F., G. J. Gu, J.-J. Wang, G. J. Huffman, S. Curtis, and D. Bolvin, 2008: Relationships between global precipitation and surface temperature on interannual and longer timescales (1979-2006). *J. Geophys. Res.*, **113**, D22104, doi:10.1029/2008JD010536.

Adler, R. F., J. -J. Wang, G. Gu, and G. J. Huffman, 2009: A ten-year Tropical Rainfall Climatology based on a composite of TRMM products. *J. Meteor. Soc. Japan*, **87A**, 281-293.

Akiyama, S., S. Shige, M. K. Yamamoto, and T. Iguchi, 2019: Heavy ice precipitation band in an oceanic extratropical cyclone observed by GPM/DPR: 1. A case study. *Geophys. Res. Lett*., **46**. https://doi.org/10.1029/2019GL082896.

Anagnostou, E. N., C. A. Morales, and T. Dinku, 2001: The use of TRMM Precipitation Radar observations in determining ground radar calibration biases. *J. Atmos. Oceanic Technol.*, **18**, 616-628.

Aoki, S., and S. Shige, 2021: Large precipitation gradients along the south coast of Alaska revealed by spaceborne radars. *J. Meteor. Soc. Japan*, **99**, https://doi.org/10.2151/jmsj.2021-001.

Aonashi, K., J. Awaka, M. Hirose, T. Kozu, T. Kubota, G. Liu, S. Shige, S. Kida, S. Seto, N. Takahashi and Y. N. Takayabu, 2009: GSMaP passive microwave precipitation retrieval algorithm: Algorithm description and validation. *J. Meteor. Soc. Japan*, **87A**, 119-136.

Aonashi, K., and H. Eito, 2011: Displaced Ensemble variational assimilation method to incorporate microwave imager data into a cloud-resolving model. *J. Meteor. Soc. Japan*, **89**, 175-194.

Aonashi, K., and T. Kubota, 2014: Experimental assimilation of the GPM core observatory DPR reflectivity profiles for Typhoon Halong. *Mon. Wea. Rev*., **144**, 2307-2326.

Atlas, D., and C. W. Ulbrich, 1977: Path- and area-integrated rainfall measurement by microwave attenuation in the 1-3 cm band, *J. Appl. Meteor.*, **16**, 1322-1331.

Atlas, D., and O. Thiele, 1981: Precipitation measurements from space, Workshop report, NASA Goddard Space Flight Center, https://ntrs.nasa.gov/citations/19830016998.

Awaka, J., T. Iguchi, and K. Okamoto, 2009: TRMM PR standard algorithm 2A23 and its performance on bright band detection. *J. Meteor. Soc. Japan*, **87A**, 31–52.

Awaka, J., M. Le, V. Chandrasekar, N. Yoshida, T. Higashiuwatoko, T. Kubota, and T. Iguchi, 2016: Rain type classification algorithm module for GPM Dual-Frequency Precipitation Radar. *J. Atmos. Oceanic Technol*., **33**, 1887–1898, https://doi.org/10.1175/JTECH-D-16-0016.1.

Battaglia, A., C. Kummerow, D.-B. Shin, and C. Williams, 2003: Constraining microwave brightness temperatures by radar brightband observations. *J. Atmos. Oceanic Technol.*, **20**, 856-871, doi:10.1175/1520-0426(2003)020.

Battaglia, A., and C. Simmer, 2008: How does multiple scattering affect the spaceborne W-band radar measurements at ranges close to and crossing the sea-surface range? *IEEE Trans. Geosci. Remote Sens.*, **46**(6), 1644-1651.

Battaglia, A., S. Tanelli, K. Mroz, and F. Tridon, 2015; Multiple scattering in observations of the GPM dual‐frequency precipitation radar: Evidence and impact on retrievals. *J. Geophys. Res. Atmos.*, **120**, 4090– 4101. doi:10.1002/2014JD022866.

Battaglia, A., P. Kollias, R. Dhillon, R. Roy, S. Tanelli, K. Lamer, M. Grecu, M. Lebsock, D. Watters, K. Mroz, G. Heymsfield, L. Li, and K. Furukawa, 2020: Spaceborne cloud and precipitation radars: Status, challenges, and ways forward. *Rev. Geophys.*, **58**, e2019RG000686.

Battan, L. J., 1973: *Radar Observation of the Atmosphere*. Univ. Chicago Press, pp. 324.

Berg, W., C. Kummerow, and C. A. Morales, 2002: Differences between east and west Pacific rainfall systems. *J. Climate*, **15**, 3659-3672, doi:10.1175/1520-0442(2002)015<3659:DBEAWP>2.0.CO;2.

Bhatt, C. B., and K. Nakamura, 2005: Characteristics of monsoon rainfall around the Himalayas revealed by TRMM precipitation radar. *Mon. Wea. Rev*. **133**, 149-165.

Bhatt, B. C., and K. Nakamura, 2006: A climatological-dynamical analysis associated with precipitation around the southern part of the Himalayas. *J. Geophys. Res.*, **111**, D02115, doi:10.1029/2005JD006197.

Bjerknes, J., 1966: A possible response of the atmospheric Hadley circulation to equatorial anomalies of ocean temperature. *Tellus*, **18**(4), 820-829.

Bjerknes, J., 1969: Atmospheric teleconnections from the equatorial Pacific. *Mon. Wea. Rev.*, **97**, 163-172.

Boukabara, S.-A., E. Jones, A. Geer, M. Kazumori, K. Garrett, and E. Maddy, 2020: Assimilation of precipitation observations from space into numerical weather prediction (NWP). In: *Satellite Precipitation Measurement*, V. Levizzani, C. Kidd., D. B. Kirschbaum, C. D. Kummerow, K. Nakamura, F. J. Turk, Eds., Springer Nature, Cham*, Advances in Global Change Research*, **69**, 941-982, https://doi.org/10.1007/978-3-030-35798-6_24.

Cecil, D. J., and E. J. Zipser, 1999: Relationships between tropical cyclone intensity and satellite-based indicators of inner core convection: 85-GHz ice-scattering signature and lightning. *Mon. Wea. Rev.*, **127**, 103-123.

Dorman, C. E., and R. H. Bourke, 1979: Precipitation over the Pacific Ocean, 30S to 60N. *Mon. Wea. Rev.*, **107**, 896-910.

De Meyer, V., and R. Roca, 2021: Thermodynamics scaling of extreme daily precipitation over the tropical ocean from satellite observations. *J. Meteor. Soc. Japan*, **99**, in press.

Durden, S. L., L. Li, E. Im, and S. H. Yueh, 2003: A surface reference technique for airborne Doppler radar measurements in hurricanes. *J. Atmos. Oceanic Technol.*, **20,** 269–275, 2003.

Elsaesser, G. S., C. D. Kummerow, and T. S. L'Ecuyer, Y. N. Takayabu, and S. Shige, 2010: Observed self-similarity of precipitation regimes over the tropical oceans. *J. Climate*, **23**, 2686-2698.

Fu, Y., and G. Liu, 2001: The variability of tropical precipitation profiles and its impact on microwave brightness temperatures as inferred from TRMM data. *J. Appl. Meteor.*, **40**, 2130–2143.

Fujinami, H., T. Sato, H. Kanamori, and F. Murata, 2017: Contrasting features of monsoon precipitation around the Meghalaya Plateau under westerly and easterly regimes. *J. Geophys. Res*. *Atmos.,* **122***,* 9591-9610, doi:10.1002/2016JD026116.

Furuzawa, F. A., and K. Nakamura, 2005: Difference of rainfall estimates over land by Tropical Rainfall Measuring Mission (TRMM) Precipitation Radar (PR) and TRMM Microwave Imager (TMI)-Dependence on storm height. *J. Appl. Meteor.* **44**, 367-383.

Gogineni, S. P., and R. K. Moore, 1989: Rain radars for earth science geostationary platforms: Some possibilities. *Earth Science Geostationary Platform Technology,* NASA Langley Research Center, 191-200.

Grossman, R., and O. Garcia, 1990: The distribution of deep convection over ocean and land during the Asian summer monsoon. *J. Climate*, **3**, 1032–1044, doi:10.1175/1520-0442(1990)003,1032:TDODCO.2.0.CO;2.

Gu., G., R. F. Adler, G. J. Huffman, and S. Curtis, 2007: Tropical rainfall variability on interannual-to-interdecadal and longer time scales derived from the GPCP monthly product. *J. Climate*, **20**, 4033-4046.

Hamada, A., Y. N. Takayabu, C. Liu, and E. J. Zipser, 2015: Weak linkage between the heaviest rainfall and tallest storms. *Nature Commun.*, **6**, 6213, doi:10.1038/ncomms7213.

Hamada, A., and Y. N. Takayabu, 2016: Improvements in detection of light precipitation with the Global Precipitation Measurement dual frequency precipitation radar (GPM DPR). *J. Atmos. Oceanic Technol.*, **33**, 653–667, doi:10.1175/JTECH-D-15-0097.1.

Hamid, E. Y., Z-I. Kawasaki, and R. Mardiana, 2001: Impact of the 1997-98 El Niño event of lightning activity over Indonesia. *Geophys. Res. Lett*., **28**, 1, pp.147-150, 2001.

Hanado, H., S. Satoh, N. Takahashi, T. Iguchi, T. Kozu, and K. Nakamura, 1998: Preliminary results of Ishigaki/Miyako Campaign Experiment for TRMM (IMCET). *Proc. IEEE Geosci. Remote Sens.*, 740-741, doi:10.1109/IGARSS.1998.699568.

Hirose, H., S. Shige, M. K. Yamamoto, and A. Higuchi, 2019: High temporal rainfall estimations from Himawari-8 multiband observations using the random-forest machine-learning method, *J. Meteor. Soc. Japan*, **97**, 689-710, https://doi.org10.2151/jmsj.2019-040.

Hirose, M., and K. Nakamura, 2002: Spatial and seasonal variation of rain profiles over Asia observed by spaceborne precipitation radar. *J. Climate,* **15** (23), 3443-3458.

Hirose, M., and K. Nakamura, 2004: Spatiotemporal variation of the vertical gradient of rainfall rate observed by the TRMM Precipitation Radar. *J. Climate*, **17**(17), 3378-3397.

Hirose, M., and K. Nakamura, 2005: Spatial and diurnal variation of precipitation systems over Asia observed by the TRMM Precipitation Radar. *J. Geophys. Res.*, **D110**, D05106, 10.1029/2004JD004815.

Hirose, M., R. Oki, S. Shimizu, M. Kachi, and T. Higashiuwatoko, 2008: Finescale diurnal rainfall statistics refined from eight years of TRMM PR data. *J. Appl. Meteor. Climatol.*, **47**, 544-561, doi:10.1175/2007JAMC1559.1.

Hirose, M., S. Shimizu, R. Oki, T. Iguchi, D. A. Short, and K. Nakamura, 2012: Incidence-angle dependency of TRMM PR rain estimates. *J. Atmos. Oceanic Technol.*, **29**(2), 192-206, doi:10.1175/JTECH-D-11-00067.1.

Hirose, M., Y. N. Takayabu, A. Hamada, S. Shige, and M. K. Yamamoto, 2017: Spatial contrast of geographically induced rainfall observed by TRMM PR. *J. Climate*, **30**, 4165-4184.

Hirose, M., and K. Okada, 2018: A 0.01 degree resolving TRMM precipitation climatology. *J. Appl. Meteor. Climatol.,* **57**(8), doi:10.1175/JAMC-D-17-0280.1.

Hiroshima, K., K. Nakamura, T. Nakazawa, and T. Kozu, 1998: Initial images of Precipitation Radar aboard Tropical Rainfall Measuring Mission (TRMM) satellite. *Tenki*, **45**, 2-3 (in Japanese).

Histchfeld, W., and J. Bordan, 1954: Errors inherent in the radar measurement of rainfall at attenuating wavelength. *J. Meteor.*, **11**, 58-67.

Hoshino, S., and T. Nakazawa, 2007: Estimation of tropical cyclone intensity using TRMM/TMI brightness temperature data. *J. Meteor. Soc. Japan*, **85**, 437-454.

Hou, A. Y., K. R. Kakar, S. Neeck, A. Azarbarzin, C. D. Kummerow, M. Kojima, R. Oki, K. Nakamura, and T. Iguchi, 2014: The Global Precipitation Measurement Mission. *Bull. Amer. Meteor. Soc*., **95**(5), 701-722.

Houze, R. A., Jr., 1977: Structure and dynamics of a tropical squall-line system. *Mon. Wea. Rev*., **105**, 1540–1567.

Houze, R. A., Jr. 1997: Stratiform precipitation in regions of convection: A meteorological paradox? *Bull. Amer. Meteor. Soc.*, **78**, 2179-2196.

Houze, R. A., Jr., S. Brodzik, C. Schumacher, S. E. Yuter, and C. R. Williams, 2004: Uncertainties in oceanic radar rain maps at Kwajalein and implications for satellite validation. *J. Appl. Meteor.*, **43**, 1114–1132.

Houze, R. A., Jr., D. C. Wilson, and B. F. Smull, 2007: Monsoon convection in the Himalayan region as seen by TRMM Precipitation Radar. *Quart. J. Roy. Meteor. Soc.*, **133**, 1389-1411.

Houze, R. A., Jr., K. L. Rasmussen, M. D. Zuluaga, and S. R. Brodzik, 2015: The variable nature of convection in the tropics and subtropics: A legacy of 16 years of the Tropical Rainfall Measuring Mission satellite. *Rev. Geophys.*, **109**, 994-1021, https://doi.org/10.1002/2015RG000488.

Huffman, G. J., R. F. Adler, M. M. Morrissey, D. T. Bolvin, S. Curtis, R. Joyce, B. McGavock, and J. Susskind, 2001: Global precipitation at one-degree daily resolution from multisatellite observations. *J. Hydrometeor.*, **2**, 36–50, doi:10.1175/1525-7541(2001)002,0036:GPAODD.2.0.CO;2.

Huffman, G. J., R. F. Adler, D. T. Bolvin, G. Gu, E. J. Nelkin, K. P. Bowman, Y. Hong, E. F. Stocker, and D. B. Wolff, 2007: The TRMM Multisatellite Precipitation Analysis (TMPA): Quasi-global, multiyear, combined-sensor precipitation estimates at fine scales. *J. Hydrometeor.*, **8**, 38-55, doi:10.1175/JHM560.1.

Huffman, G. J., R. F. Adler, D. T. Bolvin, and E. J. Nelkin, 2010: The TRMM Multi-satellite Precipitation Analysis (TMPA). Chapter 1, *Satellite Rainfall Applications for Surface Hydrology*, 3-22, doi:10.1007/978-90-481-2915-7.

Huffman, G. J., D. T. Bolvin, D. Braithwaite, K.-L. Hsu, R. J. Joyce, C. Kidd, E. J. Nelkin, S. Sorooshian, E. F. Stocker, J. Tan, D. B. Wolff, and P. Xie, 2020: Integrated Multi-satellite Retrievals for the Global Precipitation Measurement (GPM) Mission (IMERG). In: *Satellite Precipitation Measurement*, V. Levizzani, C. Kidd., D. B. Kirschbaum, C. D. Kummerow, K. Nakamura, F. J. Turk, Eds., Springer Nature, Cham*, Advances in Global Change Research*, **67**, 343-353, https://doi.org/10.1007/978-3-030- 24568-9_19.

Ichikawa, H., and T. Yasunari, 2006: time-space characteristics of diurnal rainfall over Borneo and surrounding oceans as observed by TRMM-PR. *J. Climate*, **19-20**, 5087-5099.

Igarashi, T., A. Kuze, S. Sobue, A. Yamamoto, K. Yamamoto, K. Oyoshi, K. Imaoka, and T. Fukuda, 2014: Japan's efforts to promote global health using satellite remote sensing data from the Japan Aerospace Exploration Agency for prediction of infectious diseases and air quality. *Geospatial Health*, **8**(3), S603-S610.

Iguchi, T., T. Kozu, R. Meneghini, J. Awaka, and K. Okamoto, 2000: Rain profiling algorithm for the TRMM Precipitation Radar. *J. Appl. Meteor.*, **39**, 2038-2052.

Iguchi, T., T. Kozu, J. Kwiatkowski, R. Meneghini, J. Awaka, and K. Okamoto, 2009: Uncertainties in the rain profiling algorithm for the TRMM Precipitation Radar. *J. Meteor. Soc. Japan.*, **87A**, 1-30.

Iguchi, T., N. Kawamoto, and R. Oki, 2018: Detection of intense ice precipitation with GPM/DPR. *J. Atmos. Oceanic Technol.*, **35**, 491–502, doi:10.1175/JTECH-D-17-0120.1.

Iguchi, T., 2020: Dual-frequency Precipitation Radar (DPR) on the Global Precipitation Measurement (GPM) mission's Core Observatory. In: Satellite Precipitation Measurement, V. Levizzani, C. Kidd., D. B. Kirschbaum, C. D. Kummerow, K. Nakamura, F. J. Turk, Eds., Springer Nature, Cham*, Advances in Global Change Research*, **67**, 183-192, https://doi.org/10.1007/978-3-030-24568-9_11.

Ikai, J., and K. Nakamura, 2003: Comparison of rain rates over the ocean derived from TRMM microwave imager and precipitation radar. *J. Atmos. Oceanic Technol.*, **20**(12), 1709-1726.

Ikuta, Y., 2016: Data assimilation using GPM/DPR at JMA., WGNE Blue Book: Research Activities in Atmospheric and Ocean Modelling, No. 46, Section 1, pp. 11-12.

Ikuta, Y., K. Okamoto, and T. Kubota, 2020: One-dimensional maximum likelihood estimation for spaceborne precipitation radar data assimilation, *Q. J. Royal. Meteor. Soc.*, https://doi.org/10.1002/qj.3950.

Im, E., S. L. Durden, Y. Rahrnat-Sarnii, H. Fang, V. Cable, M. Lou, and J. Huang, 2004: Advanced geostationary radar for hurricane monitoring and studies. *Proc. 2004 IEEE Radar Conf.*, 307-311, https//doi.org/10.1109/NRC.2004.1316440.

Imaoka, K., and K. Nakamura, 2012: Statistical analysis of the life cycle of isolated tropical cold cloud systems using MTSAT-1R and TRMM data. *Mon. Wea. Rev.*, **140**, 3552-3572, doi:10.1175/MWR-D-11-00364.1.

IPCC, 2013: Climate Change 2013: The physical science basis. https://www.ipcc.ch/report/ar5/wg1/

Islam, M. N., and H. Uyeda, 2008 : Vertical variations of rain intensity in different rainy periods in and around Bangladesh derived from TRMM observations. *Int. J. Climatol.,* **28**, 273-279.

JAXA, 2018: *Rain as Seen from Space 2*, JAXA/EORC, pp. 109 (in Japanese).. Available from https://www.eorc.jaxa.jp/TRMM/museum/pamphlet/book2/pdf/Rain_as_seen_from_Space_2_s.pdf.

JAXA, 2019: How about using rain data? Case studies demonstrated by TRMM/GPM/GSMaP [Fourth Edition], available from https://www.eorc.jaxa.jp/GPM/doc/data_utilization/2019_jireishu_e.pdf.

Joyce, R. J., J. E. Janowiak, P. A. Arkin, and P. Xie, 2004: CMORPH: A method that produces global precipitation estimates from passive microwave and infrared data at high spatial and temporal resolution. *J. Hydromet.*, **5**, 487-503.

Joyce, R. J., P. Xie, Y. Yarosh, J. E. Janowiak, and P. A. Arkin, 2010: CMORPH: A “morphing” approach for high resolution precipitation product generation. Chapter 1, *Satellite Rainfall Applications for Surface Hydrology*, 23-37.

Kanemaru, K., T. Kubota, T. Iguchi, Y. N. Takayabu, and R. Oki, 2017: Development of a precipitation climate record from spaceborne precipitation radar data. Part I: Mitigation of the effects of switching to redundancy electronics in the TRMM precipitation radar. *J. Atmos. Oceanic Tech.*, doi:10.1175/JTECH-D-17-0026.1.

Kanemaru, K., T. Kubota and T. Iguchi, 2019: Improvements in the beam- mismatch correction of precipitation radar data after the TRMM orbit boost. *IEEE Trans. Geosci. Remote Sens*., **5**,(9), 7161-7169, doi:10.1109/TGRS.2019.2911990.

Kanemaru, K., T. Iguchi, T. Masaki, and T. Kubota, 2020: Estimates of spaceborne precipitation radar pulse and beam width using sea surface echo data. *IEEE Trans. Geosci. Remote Sens.*, **58**(8), 5291-5303, doi:10.1109/TGRS.2019.2963090 (in print).

Kidd, C., A. Becker, G. J. Huffman, C. L. Muller, P. Joe, G. SkofronickJackson, and D. B. Kirschbaum, 2017: So, how much of the Earth's surface is covered by rain gauges?. *Bull. Amer. Meteor. Soc*., **98**, 69–78, https://doi.org/10.1175/BAMS-D-14-00283.1.

Kidd, C., Y. N. Takayabu, G. M. Skofronick-Jackson, G. J. Huffman, S. A. Braun, T. Kubota, and F. J. Turk, 2020a: The Global Precipitation Measurement (GPM) Mission. In: *Satellite Precipitation Measurement*, V. Levizzani, C. Kidd., D. B. Kirschbaum, C. D. Kummerow, K. Nakamura, F. J. Turk, Eds., Springer Nature, Cham, *Advances in Global Change Research*, **67**, 3-23, https://doi.org/10.1007/978-3-030-24568-9_1.

Kidd, C, S. Shige, D. Vila, E. Tarnavsky, M. K. Yamamoto, V. Maggioni, B. Maseko, 2020b: The IPWG satellite precipitation validation effort. Satellite Precipitation Measurement: Volume 2,, Springer, 453-470.

Kirstetter, P.-E., Y. Hong, J. J. Gourley, and Q. Cao, 2015: Impact of sub-pixel rainfall variability on spaceborne precipitation estimation: Evaluating the TRMM 2A25 product. *Quart. J. Roy. Meteor. Soc*., **141**, 953–966, https://doi.org/10.1002/qj.2416.

Kobayashi, K., S. Shige, and M. K. Yamamoto, 2018: Vertical gradient of stratiform radar reflectivity below the bright band from the tropics to the extratropical latitudes seen by GPM. *Q. J. R. Meteorol. Soc.*, **144** (Suppl. 1), 165-175, doi:10.1002/qj.3271.

Kondo, Y., A. Higuchi, and K. Nakamura, 2006: Small scale cloud activity over the maritime continent and the western Pacific as revealed by satellite data. *Mon. Wea. Rev*., **134**(6), 1581-1599.

Kodama, Y.-M., A. Ota, M. Katsumata, S. Mori, S. Satoh, and H. Ueda, 2005: Seasonal transition of predominant precipitation type and lightning activity over tropical monsoon areas derived from TRMM observations. *Geophys. Res. Letts.*, **32**, L14710, doi:10.1029/2005GL022986.

Kojima, M., T. Miura, K. Furukawa, Y. Hyakusoku, T. Ishikiri, H. Kai, T. Iguchi, H. Hanado, and K. Nakagawa, 2012: Dual-frequency precipitation radar (DPR) development on the global precipitation measurement (GPM) core observatory, *Proc. SPIE* 8528, Earth Observing Missions and Sensors: Development, Implementation, and Characterization II, 85281A, doi:10.1117/12.976823.

Kotsuki, S., K. Terasaki, and T. Miyoshi, 2014: GPM/DPR precipitation compared with a 3.5-km-resolution NICAM simulation. *SOLA*, **10**, 204-209. doi:10.2151/sola.2014-043.

Kotsuki, S., T. Miyoshi, K. Terasaki, G.-Y. Lien, and E. Kalnay, 2017: Assimilating the Global Satellite Mapping of Precipitation Data with the Nonhydrostatic Icosahedral Atmospheric Model NICAM. *J. Geophys. Res.*, **122**, 631-650. doi:10.1002/2016JD025355.

Kotsuki, S., K. Terasaki, K. Kanemaru, M. Satoh, T. Kubota, and T. Miyoshi, 2019: Predictability of record-breaking rainfall in Japan in July 2018: Ensemble forecast experiments with the Near-real-time Global Atmospheric Data Assimilation System NEXRA. *SOLA*, **15A**, 1-7. doi:10.2151/sola.15A-001.

Kozu, T., and K. Nakamura, 1991: Rainfall parameter estimation from dual-radar measurements combining reflectivity profile and path-integrated attenuation. *J. Atmos. Oceanic Technol.*, **8**(2), 260-270.

Kozu, T., T. Kawanishi, H. Kuroiwa, M. Kojima, K. Oikawa, H. Kumagai, K. Okamoto, M. Okumura, H. Nakatsuka, and K. Nishikawa, 2001: Development of precipitation radar onboard the Tropical Rainfall Measuring Mission (TRMM) satellite *IEEE Trans. Geosci. Remote Sens.*, **39**, 102-116.

Kozu, T., T. Iguchi, T. Kubota, N. Yoshida, S. Seto, J. Kwiatkowski, and Y. N. Takayabu, 2009a: Feasibility of raindrop size distribution parameter estimation with TRMM precipitation radar. *J. Meteor. Soc. Japan*, **87A**, 53-66.

Kozu, T., T. Iguchi, T. Shimomai, and N. Kashiwagi, 2009b: Raindrop size distribution modeling from a statistical rain parameter relation and its application to the TRMM Precipitation Radar rain retrieval algorithm. *J. Appl. Meteor. Climatol*., **48**, 716–724, https://doi.org/10.1175/2008JAMC1998.1.

Krishnamurti, T. N., S. Cocke, R. Pasch, and S. Low-Nam, 1983: Precipitation estimates from raingauge and satellite observations: Summer MONEX. Dept. of Meteorology, Florida State University, 373 pp.

Kubota, T., S. Shige, H. Hashizume, K. Aonashi, N. Takahashi, S. Seto, T. Ushio, K. Nakagawa, K. Iwanami, M. Kachi, and K. Okamoto, 2007: Global precipitation map using satellite-borne microwave radiometers by the GSMaP project: Production and validation. *IEEE Trans. Geosci. Remote Sens*., **45**, 2259-2275.

Kubota, T., T.Iguchi, M. Kojima, L. Liao, T. Masaki, H. Hanado, R. Meneghini, and R. Oki, 2016: A statistical method for reducing sidelobe clutter for the Ku-band precipitation radar onboard the GPM Core Observatory. *J. Atmos. Oceanic Technol.*, **33**(7), 1413-1428.

Kubota T., K. Aonashi, T. Ushio, S. Shige, Y. N. Takayabu, T. Tashima, T. Masaki, N. Kawamoto, T. Mega, M. K. Yamamoto, M. Yamaji, G. Liu, and R. Oki, 2020: Global Satellite Mapping of Precipitation (GSMaP) products in the GPM era. In: *Satellite Precipitation Measurement.* V. Levizzani, C. Kidd C., D. B. Kirschbaum, C. D. Kummerow, K. Nakamura, F. Turk (eds), *Advances in Global Change Research*, **67**, Springer, Cham. https://doi.org/10.1007/978-3-030-24568-9_20.

Kuettner, J. P., 1974: General description and central program of GATE. *Bull. Amer. Meteor. Soc.*, **55**, 712-719.

Kuleshov, Y., T. Kuboto, T. Tashima, P.-P. Xie, T. Kurino, P. Hechler, and L. V. Alexander, 2020: WMO space-based weather and climate extremes monitoring demonstration project for East Asia and Western Pacific, *WMO Bulletin*, **69**(1), 60-66.M.

Kummerow, C., W. Barnes, T. Kozu, J. Shuie, and J. Simpson, 1998: The Tropical Rainfall Measuring Mission (TRMM) sensor package. *J. Atmos. Oceanic Technol.*, **15**, 809-816.

Kummerow, C., and coauthors, 2000: The status of the Tropical Rainfall Measuring Mission (TRMM) after 2 years in orbit. *J. Appl. Meteor.*, **39**, 1965-1982.

Kummerow, C., Y. Hong, W. S. Olson, S. Yang, R. F. Adler, J. McCollum, R. Ferraro, G. Petty, D.-B. Shin, and T. T. Wilheit, 2001: The evolution of the Goddard Profiling Algorithm (GPROF) for rainfall estimation from passive microwave sensors. *J. Appl. Meteor.*, **40**, 1801-1820.

Kummerow, C. D., S. Tanelli, N. Takahashi, K. Furukawa, M. Klein, and V. Levizzani, 2020: Plans for future missions. In: *Satellite Precipitation Measurement*, V. Levizzani, C. Kidd., D. B. Kirschbaum, C. D. Kummerow, K. Nakamura, F. J. Turk, Eds., Springer Nature, Cham, *Advances in Global Change Research*,**67**, 99-119, https://doi.org/10.1007/978-3-030-24568- 9_6.

Le, M., and V. Chandrasekar, 2013a: Precipitation type classification method for dual frequency precipitation radar (DPR) onboard the GPM. IEEE Trans. *Geosci. Remote Sens.*, **51**(3), 1784–1790.

Le, M., and V. Chandrasekar, 2013b: Hydrometeor profile characterization method for dual frequency precipitation radar onboard the GPM. *IEEE Trans. Geosci. Remote Sens.*, **51**, 3648–3658.

Levizzani, V., P. Bauer, and F. J. Turk, Eds., 2007: *Measuring Precipitation from Space*, Springer, *Advances in Global Change Research*, **28**, ISBN: 978-1-4020-5834-9, 724 pp., https://doi.org/10.1007/978-1-4020-5835-6.

Levizzani, V., C. Kidd., D. B. Kirschbaum, C. D. Kummerow, K. Nakamura, and F. J. Turk, Eds., 2020a: *Satellite Precipitation Measurement,* vol. 1, Springer Nature, Cham, *Advances in Global Change Research,* **67**, ISBN: 978-3-030-24567-2, 450 pp, https://doi.org/10.1007/978- 3-030-24568-9.

Levizzani, V., C. Kidd., D. B. Kirschbaum, C. D. Kummerow, K. Nakamura, and F. J. Turk, Eds., 2020b: *Satellite Precipitation Measurement*, vol. 2, Springer Nature, Cham, *Advances in Global Change Research*, **69**, ISBN: 978-3-030-35797-9, 712 pp, https://doi.org/10.1007/978- 3-030-35798-6.

Li, J., and K. Nakamura, 2002: Characteristics of the mirror image of precipitation observed by the TRMM precipitation radar. *J. Atmos. Oceanic Technol.*, **19**(2), 145-158.

Liao, L., R. Meneghini, A. Tokay, and H. Kim, 2020: Assessment of Ku- and Ka-band Dual-frequency radar for snow retrieval. *J. Meteor. Soc. Japan*, **98**, 1129-1146.

Liu, C., E. J. Zipser, and S. W. Nesbitt, 2007: Global distribution of tropical deep convection: Different perspectives from TRMM infrared and radar data. *J. Climate*, **20**, 489–503, doi:10.1175/JCLI4023.1.

Madden R. A, and P. R. Julian, 1971: Detection of a 40–50-day oscillation in the zonal wind in the tropical Pacific. *J. Atmos. Sci.*, **28**, 702–708.

Madden R. A, and P. R. Julian, 1972: Description of global-state circulation cells in the tropics with a 40–50-day period. *J. Atmos. Sci*., **29**, 1109–1123.

Makihara, Y., 1996: A method for improving radar estimates of precipitation by comparing data from radars and raingauges. *J. Meteor. Soc. Japan,* **74,** 459–480.

Marshall, J. S., and M. Palmer, 1948: The distribution of raindrops with size. *J. Meteor.*, **5**, 165-166.

Mapes, B. E., and R. A. Houze, Jr., 1995: Diabatic divergence profiles in western Pacific mesoscale convective systems. *J. Atmos. Sci.*, **52**, 1807–1828.

Masaki, T., T. Iguchi, K. Kanemaru, K. Furukawa, N. Yoshida, T. Kubota, and R. Oki, 2020: Calibration of the Dual-frequency Precipitation Radar (DPR) onboard the Global Precipitation Measurement (GPM) core observatory, *IEEE Trans. Geosci. Remote Sens*., https://doi.org/10.1109/TGRS.2020.3039978.

Masunaga, H., T. Iguchi, R. Oki, and M. Kachi, 2002: Comparison of rainfall products derived from TRMM Microwave imager and precipitation radar. *J. Applied Meteor.*, **41**, 849-862, https://doi.org/10.11751520-0450(2002)041<0849:CORDPDF>2.0.CO;2.

S

Masunaga, H., T. S. L'Ecuyer and C. D. Kummerow, 2005: Variability in the characteristics of precipitation systems in the tropical Pacific. Part I. Spatial structure. *J. Climate*, **18**, 823-

840, doi:10.1175/JCLI-3304.1.

Masunaga, H., T. S. L'Ecuyer, and C. D. Kummerow, 2006: The Madden-Julian Oscillation recorded in early observations from the Tropical Rainfall Measuring Mission (TRMM). *J. Atmos. Sci*., **63**, 2777-2794.

Masunaga, H. 2012: A satellite study of the atmospheric forcing and response to moist convection over tropical and subtropical oceans. *J. Atmos. Sci.* **69**, 150-167.

Masunaga, H. 2013: A satellite study of the atmospheric forcing and response to moist convection over tropical convection and environmental variability. *J. Atmos. Sci.* **70**, 2443-2466.

Masunaga, H., and Z. J. Luo, 2016: Convective and large-scale mass flux profiles over tropical oceans determined from synergistic analysis of a suite of satellite observations. *J. Geophys. Res. Atmos.*, **121,** doi:10.1002/2016JD024753.

Matsuno, T. 2016: Prologue: Tropical meteorology 1960–2010—Personal recollections. Multiscale Convection–Coupled Systems in the Tropics: A Tribute to Dr. Michio Yanai, *Meteor. Monogr.*, **56**, Amer. Meteor. Soc., vii–xv, doi:.10.1175/AMSMONOGRAPHS-D-15-0012.1.

Mega, T., T. Ushio, T. Matsuda, M. Kachi, and R. Oki, 2019: Gauge-adjusted Global Satellite Mapping of Precipitation. *IEEE Trans. Geosci. Remote Sens.*, **57**(4), 1928-1935, doi:10.1109/TGRS.2018.2870199.

Medina, S., R. A. Houze, Jr., A. Kumar, and D. Niyogi, 2010: Summer monsoon convection in the Himalayan region: Terrain and land cover effects. *Quart. J. Roy. Meteor. Soc.*, **136**, 593-616.

Meneghini, R., 1978: Rain-rate estimates for an attenuating radar. *Radio Sci.*, **13**, 459-470, doi:10.1029/RS013i003p00459.

Meneghini, R., J. Eckerman and D. Atlas, 1983: Determination of rain rate from a spaceborne radar using measurements of total attenuation. *IEEE Trans. Geosci. Remote Sens*., **21**, 34-43. doi:10.1109/TGRS.1983.350528.

Meneghini, R., and D. Atlas, 1986: Simultaneous ocean cross section and rainfall measurements from space with a nadir-looking radar. *J. Atmos. Oceanic Technol.*, **3**, 400–413.

Meneghini, R., T. Iguchi, T. Kozu, L. Liao, K. Okamoto, J. A. Jones, and J. Kwiatkowski, 2000: Use of the surface reference technique for path attenuation estimates from TRMM Precipitation Radar. *J. Appl. Meteor.,* **39**, 2053-2070.

Meneghini. R., L. Liao, S. Tanelli, and S. L. Durden, 2012: Assessment of the performance of a dual-frequency surface reference technique over ocean. *IEEE Trans. Geosci. Remote Sens.*, **50**(8), 2968-2977.

Meneghini, R., H. Kim, L. Liao, J. A. Jones, and J. M. Kwiatkowski, 2015: An initial assessment of the surface reference technique applied to data from the dual-frequency precipitation radar (DPR) on the GPM satellite. *J. Atmos. Oceanic Technol*., **32**, 2281-2296.

Meneghini, R., H. Kim, L. Liao, J. Kwiatkowski, and T. Iguchi: Path attenuation estimates for the GPM Dual-Frequency Precipitation Radar (DPR). *J. Meteor. Soc. Japan,* **99**, in press.

Miyoshi, T., S. Kotsuki, K. Terasaki, S. Otsuka, G.-Y. Lien, H. Yashiro, H. Tomita, M. Satoh, and E. Kalnay, 2020: Precipitation ensemble data assimilation in NWP models. In: *Satellite Precipitation Measurement*, V. Levizzani, C. Kidd., D. B. Kirschbaum, C. D. Kummerow, K. Nakamura, F. J. Turk, Eds., Springer Nature, Cham, *Advances in Global Change Research*, **69**, 983-991, https://doi.org/10.1007/978-3-030-35798-6_25.

Mori, S., J. Hamada, Y. I. Tuhid, and M. D. Yamanaka, 2004: Diurnal land-sea rainfall peak migration over Sumatera Island, Indonesian Maritime Continent, observed by TRMM satellite and intensive rawinsonde soundings. *Mon. Wea. Rev.*, **132**, 2021-2039.

Mori, T., S. Nakamura, and M. Yamaji, 2020: Potential use of Global Satellite Mapping of Precipitation (GSMaP) for river runoff estimation in hydropower development studies. *Electric Power Civil Engineering*, **410**, 57-61 (In Japanese).

National Academies of Sciences, Engineering, and Medicine, 2019: *Thriving on Our Changing Planet: A decadal Strategy for Earth Observation from Space: An Overview for decision Makers and the Public*, Washington, DC: The National Academies Press, https://doi.org/10.17226/25437.

Nakamura, K., K. Okamoto, T. Ihara, J. Awaka, T. Kozu, and T. Manabe, 1990: Conceptual design of rain radar for the Tropical Rainfall Measuring Mission. *Int. J. Sat. Commun.*, **8**, 257-268.

Nakamura, K., 1991: Biases of rain retrieval algorithms for spaceborne radar caused by nonuniformity of rain. *J. Atmos. Oceanic Technol.*, **8**(3), 363-373.

Nakamura, K., Y. Kaneko, K. Nakagawa, H. Hanado, and M. Nishikawa, 2018: Measurement method for specific attenuation in the melting layer using a dual Ka-band radar system. *IEEE Trans. Geosci. Remote Sens.*, **56**(6), 3511-3519, doi:10.1109/TGRS.201801291.

Nesbitt, S. W., and E. J. Zipser, 2003: The diurnal cycle of rainfall and convective intensity according to three years of TRMM measurements. *J. Climate*, **16**, 1456–1475.

Nguyen, P., M. Ombadi, S. Sorooshian, K. Hsu, A. AghaKouchak, D. Braithwaite, H. Ashouri, and A R. Thorstensen, 2018: The PERSIANN family of global satellite precipitation data: A review and evaluation of products. *Hydrol. Earth Syst. Sci.*, **22**, 5801-5816.

Ninomiya, K., 1984: Characteristics of Baiu front as a predominant subtropical front in the summer northern hemisphere. *J. Meteor. Soc. Japan*, **62**, 880-894.

Nishikawa, M, K. Nakamura, Y. Fujiyoshi, K. Nakagawa, H. Hanado, H. Minda, S. Nakai, T. Kumakura, and R. Oki, 2015: Radar attenuation and reflectivity measurements of snow with dual Ka-band radar. *IEEE Trans. Geosci. Remote Sens*., **54**(2), 714-722, doi:10.1109/TGRS.2015.2464099.

Ogino, S. Y., M. D. Yamanaka, S. Mori, and J. Matsumoto, 2016: How much is the precipitation amount over the tropical coastal region? *J. Climate*, **29**, 1231–1236.

Ogino, S. Y., M. D. Yamanaka, S. Mori, and J. Matsumoto, 2017: Tropical coastal dehydrator in global atmospheric water circulation. *Geophys. Res. Lett*., **44**, 11636-11643.

Okamoto, K., A Short History of the TRMM Precipitation Radar. *Meteor. Monogr*., 2003; **51** 187–195. doi: https://doi.org/10.1175/0065- 9401(2003)0292.0.CO;2.

Okamoto, K., K. Aonashi, T. Kubota, T. Tashima, 2016: Experimental assimilation of the GPM-Core DPR reflectivity profiles for Typhoon Halong, *Mon. Wea. Rev.*, **144** (6), 2307-2326.

Okazaki, A., T. Honda, S. Kotsuki, M. Yamaji, T. Kubota, R. Oki, T. Iguchi, and T. Miyoshi, 2019: Simulating precipitation radar observations from a geostationary satellite, *Atmos. Measurement Tech.*, **12,** 3985- 3996, doi:10.5194/amt-12-3985-2019.

Oyoshi, K., K. Kobayashi, T. Muto, T. Okumura, S. Sobue, and Y. Kaneko, 2016:, Development of an agrometeorological data provision system for the outlook of rice growth and production in Asia, *J. Japan Soc. Photogrammetry Remote Sens.*, **55**(3), 200-205, https://doi.org/10.4287/jsprs.55.200 (in Japanese).

Peral, E., S. Tanelli, S. Statham, S. Joshi, T. Imken, D. Price, J. Sauder, N. Chahat, and A. Williams, 2019: RainCube: the first ever radar measurements from a CubeSat in space. *J. Applied Remote Sens.*, **13**(3) 032504, doi:10.1117/1.JRS.13.032504.

Petersen, W. A., and S. A. Rutledge, 2001: Regional variability in tropical convection: Observations from TRMM. *J. Climate*, **14,** 3566–3586.

Petersen, W. A., S. W. Nesbitt, R.J. Blakeslee, R. Cifelli, P. Hein, and S. A. Rutledge, 2002: TRMM observations of intraseasonal variability in convective regimes over the Amazon. *J. Climate*, **15**, 1278-1294.

Pham, N. T. T., C. T. Nguyen, D. T. Vu, and K Nakamura, 2018: Mapping of dengue vulnerability in the Mekong Delta region of Viet Nam using a water-associated disease index and remote sensing approach. *APN Sci. Bull.*, **8**(1), Sept. 2018.

Rosenfeld, D., 1999: TRMM observed first direct evidence of smoke from forest fires inhibiting rainfall. *Geophys. Res. Letts*., **26**, 3105-3108, doi:10.1029/1999GL006066.

Romatschke, U., S. Medina, and R. A. Houze, Jr., 2010: Regional, seasonal, and diurnal variations of extreme convection in the South Asian region. *J. Climate*, **23**, 419-439.

Satoh, M., T. Matsuno, H. Tomita, H. Miura, T. Nasuno, and S. Iga, 2008: Nonhydrostatic Icosahedral Atmospheric Model (NICAM) for global cloud resolving simulations. *J. Computational Phys*., **227**, 3486–3514, doi:10.1016/j.jcp.2007.02.006.

Satoh, M., H. Tomita, H. Yashiro, H. Miura, C. Kodama, T. Seiki, A. T. Noda, Y. Yamada, D. Goto, M. Sawada, T. Miyoshi, Y. Niwa, M. Hara, T. Ohno, S. Iga, T. Arakawa, T. Inoue, and H. Kubokawa, 2014: The Non-hydrostatic Icosahedral Atmospheric Model: Description and development. *Prog. in Earth and Planet. Sci.* **1,** 18, doi:10.1186/s40645-014-0018-1.

Schumacher, C., and R. A. Houze, 2000: Comparison of radar data from the TRMM satellite and Kwajalein oceanic validation site. *J. Appl. Meteor.*, **39,** 2151–2164.

Seto, S., and T. Iguchi, 2011: Applicability of the iterative backward retrieval method for the GPM Dual-frequency Precipitation Radar. *IEEE Trans. Geosci. Remote Sens.*, **49**(6), 1827–1838.

Seto, S., T. Iguchi, and T. Oki, 2013: The basic performance of a precipitation retrieval algorithm for the Global Precipitation Measurement mission’s single/dual-frequency radar measurements. *IEEE Trans. Geosci. Remote Sens*., **51**(12), 5239–5251.

Seto, S., and T. Iguchi, 2015: Intercomparison of attenuation correction methods for the GPM Dual-frequency Precipitation Radar. *J. Atmos. Oceanic Tech*., **32**(5), 915-926.

Seto, S., T. Iguchi, R. Meneghini, J. Awaka,T. Kubota, T. Masaki and N. Takahashi, 2020: The precipitation rate retrieval algorithms for the GPM Dual-frequency Precipitation Radar, *J. Meteor. Soc. Japan*, https://doi.org/10.2151/jmsj.2021-011.

Shige, S., Y. N. Takayabu, W.-K. Tao, and D. E. Johnson, 2004: Spectral retrieval of latent heating profiles for TRMM PR data. Part I: Development of a model-based algorithm. *J. Appl. Meteor.*, **43**, 1095-1113.

Shige, S., Sasaki, H., Okamoto, K., and Iguchi, T., 2006: Validation of rainfall estimates from the TRMM precipitation radar and microwave imager using a radiative transfer model: 1. Comparison of the version-5 and -6 products, *Geophys. Res. Lett.*, **33**, L13803, doi:10.1029/2006GL026350.

Shige, S., Y. N. Takayabu, W.-K. Tao, and C.-L. Shie, 2007: Spectral retrieval of latent heating profiles from TRMM PR data. Part II: Algorithm improvement and heating estimates over tropical ocean regions. *J. Appl. Meteor. Climatol.*, **46**, 1098-1124.

Shige, S., Y. N. Takayabu, and W.-K. Kuo, 2008: Spectral retrieval of latent heating profiles from TRMM PR data. Part III: Estimating apparent moisture sink profiles over tropical oceans. *J. Appl. Meteor. Climatol.*, **47**, 620-640.

Shige, S., Watanabe, T., Sasaki, H., Kubota, T., Kida, S., and K. Okamoto, 2008: Validation of western and eastern Pacific rainfall estimates from the TRMM PR using a radiative transfer model, *J. Geophys. Res.,* **113**, D15116, doi:10.1029/2007JD009002.

Shige, S., Y. N. Takayabu, S. Kida, W.-K. Tao, X. Zeng, C. Yokoyama, and T. L'Ecuyer, 2009: Spectral retrieval of latent heating profiles from TRMM PR data. Part IV: Comparisons of lookup tables from two- and three-dimensional cloud-resolving model simulations. *J. Climate,* **22**, 5577-5594.

Shige, S., S. Kida, H. Ashiwake, T. Kubota, and K. Aonashi, 2013: Improvement of TMI rain retrievals in mountainous areas. *J. Appl. Meteor. Climatol*., **52,** 242-254.

Shige, S., M. K. Yamamoto, and A. Taniguchi, 2014: Improvement of TMI rain retrieval over the Indian subcontinent. Remote Sensing of the Terrestrial Water Cycle, *Geophys. Monogr.,* **206**, Amer. Geophys. Union, 27–42, doi:10.1002/9781118872086.ch2.

Shige, S. and C. D. Kummerow, 2016: Precipitation-top heights of heavy orographic rainfall in the Asian monsoon region. *J. Atmos. Sci.,* **73**, 3009-3024, https://doi.org/10.1175/JAS-D-15-0271.1.

Shige, S., Y. Nakano, and M. K. Yamamoto, 2017: Role of orography, diurnal cycle, and intraseasonal oscillation in summer monsoon rainfall over the Western Ghats and Myanmar coast. *J. Climate*, **30**, 9365–9381, https://doi.org/10.1175/JCLI-D-16-0858.1

Shimizu, S., R. Oki, T. Tagawa, T. Iguchi, and M. Hirose, 2009: Evaluation of the effects of the orbit boost of the TRMM satellite on PR rain estimates. *J. Meteor. Soc. Japan*, **87A**, 83-92, doi:10.2151/jsj.87A.83.

Short, D., and K. Nakamura, 2000: TRMM radar observation of shallow precipitation over the tropical oceans. *J. Climate*, **13** (23), 4107-4124.

Simpson, J., R. F. Adler, and G. R. North, 1988: A proposed Tropical Rainfall Measuring Mission (TRMM) satellite. *Bull. Amer. Meteor. Soc.*, **69**, 278-295.

Singh P., and K. Nakamura, 2009: Diurnal variation in summer precipitation over the central Tibetan Plateau, *J. Geophys. Res*., **114**, D20107, doi:10.1029/2009JD011788.

Singh, P., and K. Nakamura, 2010: Diurnal variation in summer monsoon precipitation during active and break periods over central India and southern Himalayan foothills. *J. Geophys. Res.*, **115**, D12122, doi:10.1029/2009JD012794.

Skofronick-Jackson, G., W. A. Petersen, W. Berg, C. Kidd, E. F. Stocker, D. B. Kirschbaum, R. Kakar, S. A. Braun, G. J. Huffman, T. Iguchi, P. E. Kirstetter, C. Kummerow, R. Meneghini, R. Oki, W. S. Olson, Y. N. Takayabu, K. Furukawa, and T. Wilheit, 2017: The Global Precipitation Measurement (GPM) for science and society. *Bull. Amer. Meteor. Soc.*, **98,** 1679-1695.

Sohn, B. J., H.-J. Han, and E.-K. Seo, 2010: Validation of satellite-based high-resolution rainfall products over the Korean peninsula using data from a dense rain gauge network. *J. Appl. Meteor. Climatol.*, **49**, 701–714, doi:10.1175/2009JAMC2266.1.

Sohn, B. J., G.-H. Ryu, H.-J. Song, and M.-L. Ou, 2013: Characteristic features of warm-type rain producing heavy rainfall over the Korean peninsula inferred from TRMM measurements. *Mon. Weather Rev.*, **141**, 3873–3888, doi:10.1175/MWR-D-13-00075.1.

Song, H.-J., and B. J. Sohn, 2015: Two heavy rainfall types over the Korean peninsula in the humid East Asian summer environment: A satellite observation study. *Mon. Wea. Rev.*, **143**, 363–382, doi:10.1175/MWR-D-14-00184.1.

Sorooshian, S., K. Hsu, X. Gao, H. Gupta, B. Imam, and D. Braithwaite, 2000: Evaluation of PERSIANN System satellite-based estimates of tropical rainfall. *Bull. Amer. Meteor. Soc.*, **81**(9), 2035-2046.

Stephens, G. L., J. Li, M. Wild, C. A. Clayson, N. Loeb, S. Kato, T. L'Ecuyer, P. W. Stackhouse, Jr., M. Lebsock, and T. Andrews, 2012: An update on Earth's energy balance in light of the latest global observations. *Nature Geosci.*, **5**, 691-694.

Sumi, Y., and H. Masunaga, 2016: A moist static energy budget analysis of quasi 2-day wave using satellite and reanalysis data. *J. Atmos. Sci*., **73**, 743-759, doi:10.1175/JAS-D-1.

Takahashi, N., H. Kuroiwa, and T. Kawanishi, 2003: Four-year result of external calibration for Precipitation Radar (PR) of the Tropical Rainfall Measuring Mission (TRMM) satellite. *IEEE Trans. Geosci. Remote Sens*., **41**, 2398-2403.

Takahashi, N., H. Hanado, K. Nakamura, K. Kanemaru, K. Nakagawa, T. Iguchi, T. Nio, T. Kubota, R. Oki, and N. Yoshida, 2016: Overview of the end-of-mission observation experiments of precipitation radar onboard the Tropical Rainfall Measuring Mission satellite. *IEEE Trans. Geosci. Remote Sens.*, **54**, 3450-3459.

Takahashi, N., 2017: Surface echo characteristics derived from the wide swath experiment of the precipitation radar onboard TRMM satellite during its end-of-mission operation. *IEEE Trans. Geosci. Remote Sens.* doi:10.1109/TGRS.2016.2633971.

Takayabu, Y. N., 2002: Spectral representation of rain profiles and diurnal variations observed with TRMM PR over the equatorial area. *Geophys. Res. Letts*., **29**, 1584, doi:10.1029/2001GL014113.

Takayabu, Y. N., T. Iguchi, M. Kachi, A. Shibata, and H. Kanzawa, 1999: Abrupt termination of the 1997-98 El Nino in response to a Madden-Julian oscillation. *Nature*, **402**, 279-282.

Takayabu, Y. N., 2006: Rain-yield per flash calculated from TRMM PR and LIS data and its relationship to the contribution of tall convective rain. *Geophys. Res. Lett.*, **33**, L18705, doi:10.1029/2006GL027531.

Takayabu, Y. N., and M. Kimoto, 2008: Diurnal march of rainfall simulated in a T106 AGCM and dependence on cumulus schemes. *J. Meteor. Soc. Japan*, **86A**, 163-173.

Takayabu, Y. N., 2008: Observing rainfall regimes using TRMM PR and LIS data. *GEWEX News*, **18**(2), 9-10.

Takayabu, Y. N., S. Shige, W.-K. Tao, and N. Hirota, 2010: Shallow and deep latent heating modes over tropical oceans observed with TRMM spectral latent heating data. *J. Climate*, **23**, 2030-2046.

Taniguchi, A., S. Shige, M. K. Yamamoto, T. Mega, S. Kida, T. Kubota, M. Kachi, T. Ushio, and K. Aonashi, 2013: Improvement of high-resolution satellite rainfall product for Typhoon Morakot over Taiwan. *J. Hydrometeor.*, **14**, 1859-1871.

Takayabu, Y. N., and W.-K. Tao, 2020: Latent heating retrievals from satellite observations. In: *Satellite Precipitation Measurement,* V. Levizzani, C. Kidd., D. B. Kirschbaum, C. D. Kummerow, K. Nakamura, F. J. Turk, Eds., Springer Nature, Cham, *Advances in Global Change Research*, **69**, 897-915.

Tao, W.-K., E. A. Smith, R. F. Adler, Z. S. Haddad, A. Y. Hou, T. Iguchi, R. Kakar, T. N. Krishnamurti, C. D. Kummerow, S. Lang, R. Meneghini, K. Nakamura, T. Nakazawa, W. S. Olson, S. Satoh, S. Shige, J. Simpson, Y. N. Takayabu, G. J. Tripoli, and S. Yang, 2006: Retrieval of latent heating from TRMM measurements. *Bull. Amer. Meteor. Soc*., **87**, 1555-1572.

Tao, W.-K., Y. N. Takayabu, S. Lang, S. Shige, W. Olson, A. Hou, G. Skofronick-Jackson, X. Jiang, C. Zhang, W. Lau, T. Krishnamurti, D. Waliser, M. Grecu, P. E Ciesielski, R. H. Johnson, R. Houze, R. Kakar, K. Nakamura, S. Braun, R. Oki, and A. Bhardwaj, 2016: TRMM latent heating retrieval: Applications and comparisons with field campaigns and large-scale analyses. *Meteor. Monogr., Multi-scale convection-coupled systems in the tropics: A tribute to Dr. Michio Yanai*, **56**, 2.1-2.34, doi:10.1195/AMSMONOGRAPHS-D-15-0013.1.

Tashima, T,, T. Kubota, T. Mega, and T. Ushio, 2020: Precipitation extremes monitoring using the near-real-time GSMaP product. *IEEE J. Sel. Topics Appl. Earth Observ. Remote Sens.* (in print).

Theon, J., and N. Fugono eds., 1988: *Tropical Rainfall Measurements*. Deepak Pub., pp. 522.

Tokay, A., and D. A. Short, 1996: Evidence from tropical raindrop spectra of the origin of rain from stratiform versus convective clouds. *J. Appl. Meteor*., **35**, 355-371.

Toyoshima, K., Masunaga, H., and Furuzawa, F. A. 2015: Early evaluation of Ku- and Ka-band sensitivities for the global precipitation measurement (GPM) dual-frequency precipitation radar (DPR). *SOLA*, **11**, 14–17, https://doi.org/10.2151/sola.2015-004.

Tsuda, M., A. Sugiura, T. Sayama, and Y. Iwami, 2014: Development of a flood forecasting system on the Indus river basin, C*ivil Engineering J.* **11**, 34-37 (in Japanese).

Ushio, T., K. Sasashige, T. Kubota, S. Shige, K. Okamoto, K. Aonashi, T. Inoue, N. Takahashi, T. Iguchi, M. Kachi, R. Oki, T. Morimoto, Z. Kawasaki, 2009: A Kalman filter approach to the Global Satellite Mapping of Precipitation (GSMaP) from combined passive microwave and infrared radiometric data. *J. Meteor. Soc. Japan*, **87A**, 137-151.

Warren, R. A., A. Protat, S. T. Siems, H. A. Ramsay, V. Louf, M. J. Manton, and T. A. Kane, 2018: Calibrating ground-based radars against TRMM and GPM. *J. Atmos. Oceanic Technol.*, **35**, 323–346, https://doi.org/10.1175/JTECH-D-17-0128.1.

Webster, P. J., and R. A. Lukas, 1992: TOGA/COARE: The Coupled Ocean-Atmosphere Response Experiment. *Bull. Amer. Meteor. Soc.*, **73**, 1377-1416.

Wilheit, T. T., J. S. Theon, W. E. Shenk, L. J. Allison, and E. B. Rogers, 1976: Meteorological interpretation of the images from the Nimbus-5 electrically scanned microwave radiometer. *J. Appl. Meteor.*, **15**, 168-172.

Wilheit, T. T., A. T. C. Chang, M. S. V. Rao, E. B. Rogers, and J. S. Theon, 1977: A satellite technique for quantitatively mapping rainfall rates over the ocean. *J. Appl. Meteor.*, **16**, 551-560.

Wilheit, T. T., and A. T. C. Chang, 1980: An algorithm for retrieval of ocean's surface and atmospheric parameters from the observations of the Scanning Multichannel Microwave Radiometer. *Radio Sci.*, **15**, 65-77.

Williams, E., and coauthors, 2002: Contrasting convective regimes over the Amazon: Implications for cloud electrification *J. Geophys. Res.*, **107**(D20), 8082, doi:10.1029/2001JD000380.

Wu, H., R. F. Adler, Y. Tian, G. J. Huffman, H. Li, and J. Wang, 2014: Real-time global flood estimation using satellite-based precipitation and a coupled land surface and routing model. *Water Resour. Res.*, **50**, 2693.2717, doi:10.1002/2013WR014710.

Yamaji, M., T. Kubota and R. Oki, 2019: Observing system simulation experiment on the accuracy of Global Satellite Mapping of Precipitation (GSMAP) by future small precipitation radar constellation, *Proc. IGARSS 2019*, Yokohama, Japan, 2019, 7594-7597, doi:10.1109/IGARSS.2019.8899209.

Yamaji, M., H. Takahashi, T. Kubota, R. Oki, A. Hamada, and Y. N. Takayabu, 2020: 4-year climatology of global drop size distribution and its seasonal variability observed by spaceborne dual-frequency precipitation radar: *J. Meteor. Soc. Japan*, 98, 755-773, https://doi.org/10.2151/jmsj.2020-038.

Yamamoto, M. K., F. A. Furuzawa, A. Higuchi, and K. Nakamura, 2008: Comparison of diurnal variations in precipitation systems observed by TRMM PR, TMI, and VIRS. *J. Climate*, **21**, 4011-4028 DOI: 10.1175/2007JCLI2079.1.

Yamamoto, M. K. and S. Shige, 2015: Implementation of an orographic/nonorographic rainfall classification scheme in the GSMaP algorithm for microwave radiometers. *Atmos. Res*., **163,** 36-47, doi:10.1016/j.atmosres.2014.07.024.

Yamamoto, M. K., S. Shige, C.-K. Yu, and L.-W. Chen, 2017: Further improvement of the heavy orographic rainfall retrievals in the GSMaP algorithm for microwave radiometers. *J. Appl. Meteor. Climatol*., **56**, 2607- 2619, doi:10.1175/JAMC-D-16-0332.1.

Yamamoto, K., T. Kubota, N. Takahashi, K. Kanemaru, T. Masaki and K. Furukawa, 2020: A feasibility study on wide swath observation by spaceborne precipitation radar, *IEEE J. Sel. Topics Appl. Earth Observ. Remote Sens.*, **13**, 3047-3057, 2020, doi:10.1109/JSTARS.2020.2998724.

Yokoyama, C., and Y. N. Takayabu, 2008: A statistical study on rain characteristics of tropical cyclones using TRMM satellite data. *Mon. Wea. Rev.*, **136**, 3848-3862.

Yokoyama, C., Y. N. Takayabu, and S. Kanada, 2014: A contrast in precipitation characteristics across the Baiu front near Japan. Part I: TRMM PR observation. *J. Climate*, **27**, 5872-5890.

Yokoyama, C., T. Y. N. Takayabu, and T. Horinouchi, 2017: Precipitation characteristics over East Asia in early summer: Effects of the subtropical jet and lower-tropospheric convective instability. *J. Climate*, **20**, 8127-8147, doi:10.1175/JCLI-D-16-0724.1.

Zipser, E. J., D. J. Cecil, C. Liu, S. W. Nesbitt, and D. P. Yorty, 2006: Where are the most intense thunderstorms on Earth? *Bull. Amer. Meteor. Soc.*, **87**, 1057-1071, doi:10.1175/BAMS-87-8-1057.

List of Figures

Fig. 7. (a) Fine resolution (0.1, 0.05, and 0.01 deg.) precipitation map around Yakushima Island generated from TRMM PR data from 1998 to 2013 and (b) rain map from rain gauge data (Hirose and Okada 2018). (© American Meteorological Society. Used with permission)

Fig. 8. Storm top distribution around 35 deg. N in summer 1998 (JAXA 2018).

Fig. 9. Storm top distribution in DJF 1998 (Short and Nakamura 2000). (© American Meteorological Society. Used with permission)

Fig. 10. Dominant precipitations derived from TRMM PR data (Takayabu 2008)

Fig. 11. Global map of peak local time of precipitation for 1998-2005 derived from TRMM microwave radiometer (TMI) (Hirose et al. 2008). (© American Meteorological Society. Used with permission)

Fig. 12. Distribution of precipitation systems of 1000 – 10000 km^2 at local time of 09:00 (top) and 15:00 (bottom) in Southeast Asia in JJA for 1998 – 2003 derived from TRMM PR data (courtesy of M. Hirose. For more details, see Hirose and Nakamura 2005).

Fig. 13. Diurnal variation of precipitation over the southern slope of the Himalayas (Bhatt and Nakamura 2006).

Fig. 14. Left (A): convergence and vertical air flow derived from TOGA/COARE (Mapes and Houze 1995), and right (B): latent heating profiles suggested from the field experiment like TOGA/COARE (Houze 1995). (a) and (b) are heating rate and divergence for convective, and (c) and (d) are for stratiform. (© American Meteorological Society. Used with permission)

Fig. 15. Vertical cross section of rain rate (upper) and latent heat release (lower) for a typhoon (JAXA 2018).

Fig. 16 Top: five-year-mean KuPR precipitation frequency in western side of North America from April 2014 to March 2019 (Aoki and Shige 2021).

Fig. 17. Mass-weighted mean raindrop diameter (a) and mean precipitation rate rate (b) from GPM DPR 4-year data (Yamaji et al. 2020).

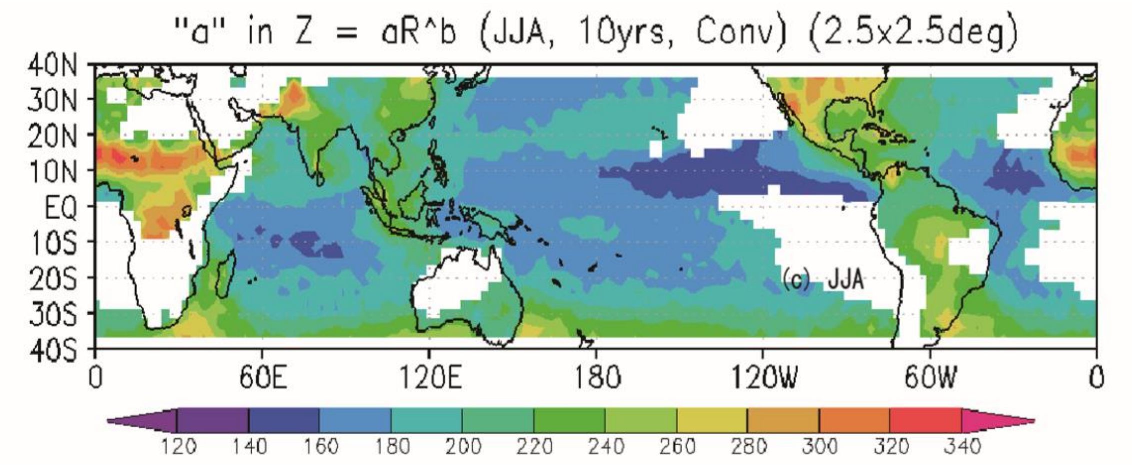

Fig. 1. Global distribution of DSD related parameters in JJA over 10 years derived from TRMM PR data (Kozu et al. 2009a).

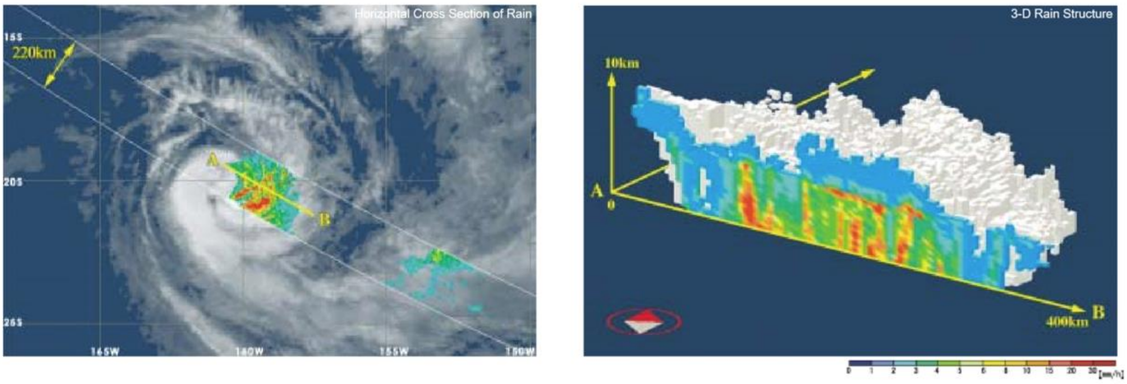

Fig. 2. 3D image of precipitation in Cyclone Pam taken by TRMM PR two weeks after the launch (Hiroshima et al. 1998).

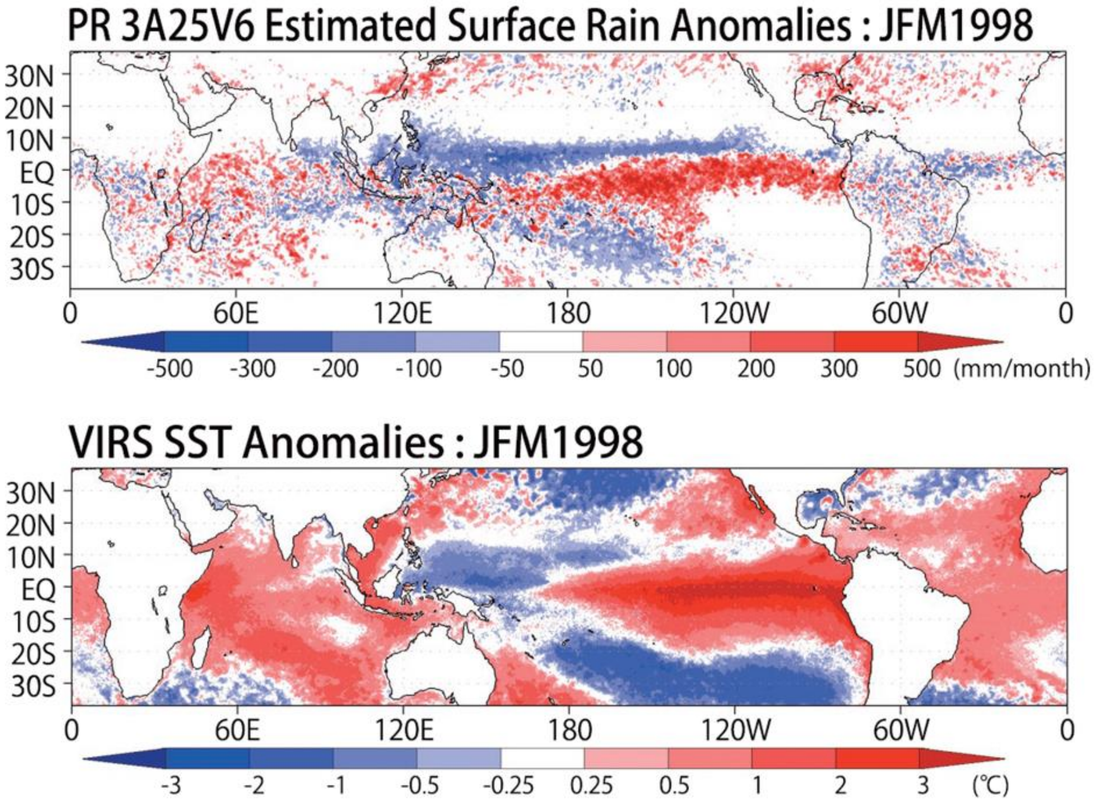

Fig. 3. Precipitation anomaly from TRMM PR data (top) and SST anomaly from TRMM VIRS data (bottom) for the El Niño (Dec. 1997- Feb. 1998 (JAXA 2018).

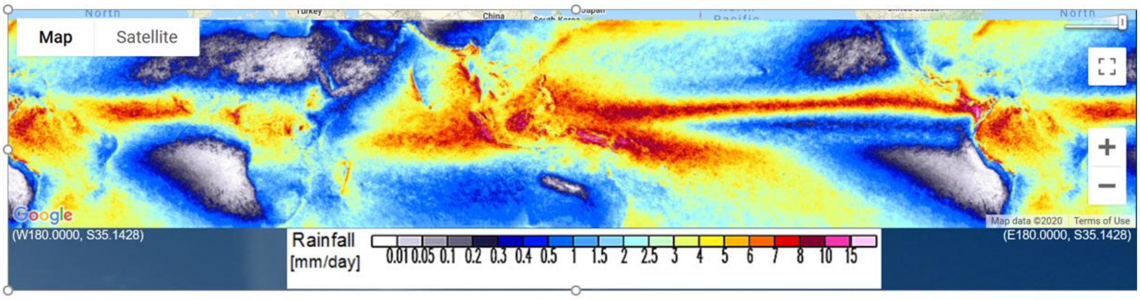

Fig. 4. Global rain distribution from TRMM PR (courtesy of M. Hirose, https://www.rain-clim.com/rainmap.html).

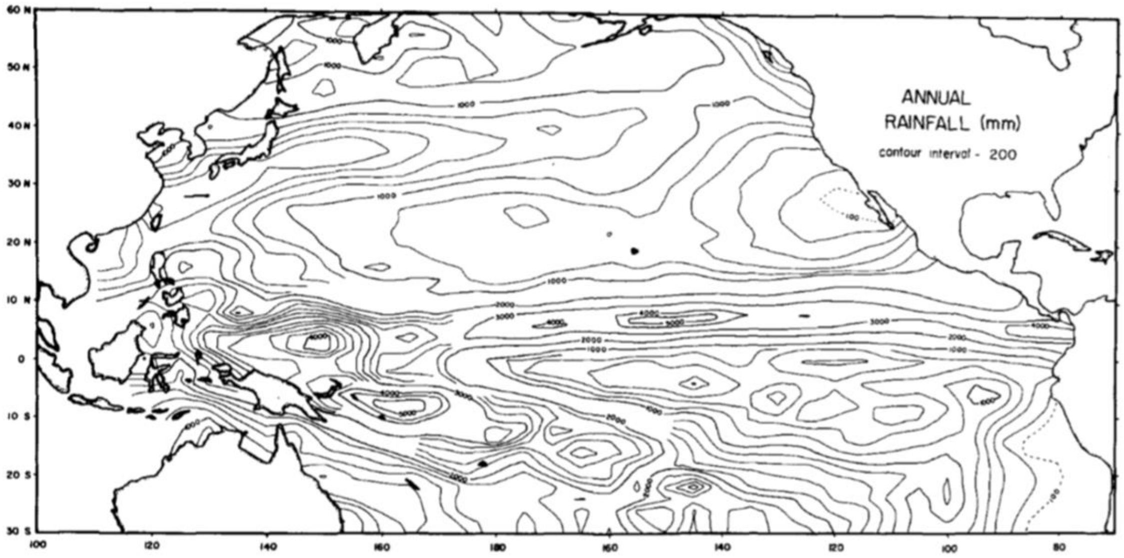

Fig. 5. Annual rain distribution from ship data for 1950-1972 (Dorman and Bourke 1979). (© American Meteorological Society. Used with permission)

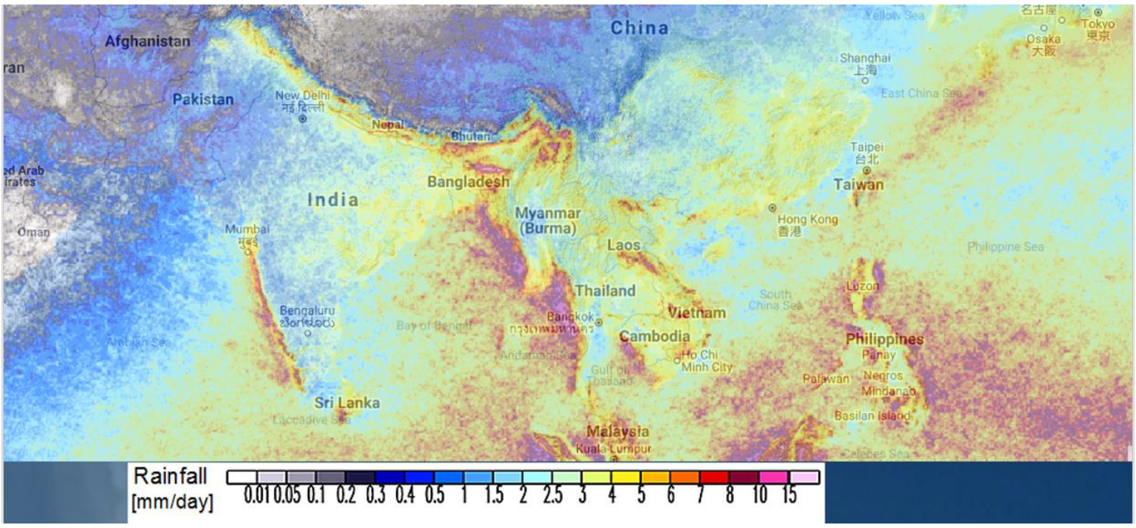

Fig. 6. Fine resolution rain distribution over Southeast Asia generated from TRMM PR data from 1998 to 2013 (courtesy of M. Hirose, https://www.rain-clim.com/rainmap.html).

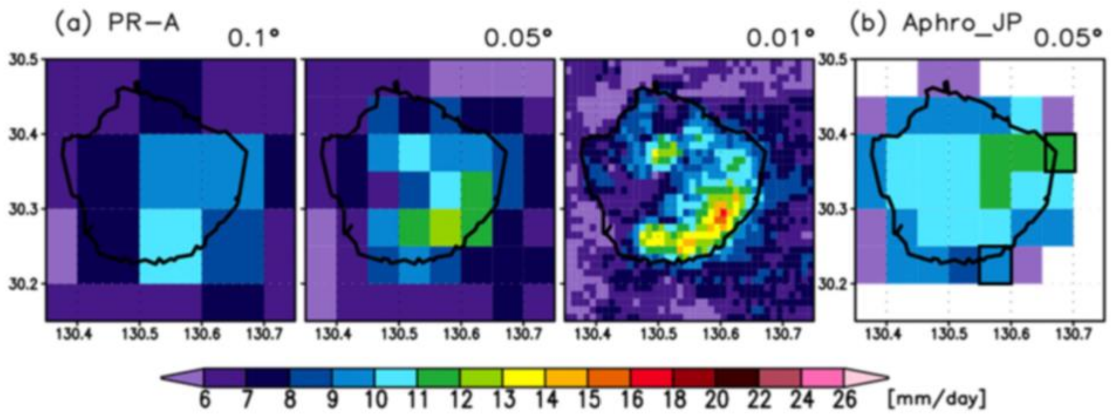

Fig. 7. (a) Fine resolution (0.1, 0.05, and 0.01 deg.) precipitation map generated from TRMM PR data from 1998 to 2013 and (b) rain map from rain gauge data (Hirose and Okada 2018). (© American Meteorological Society. Used with permission)

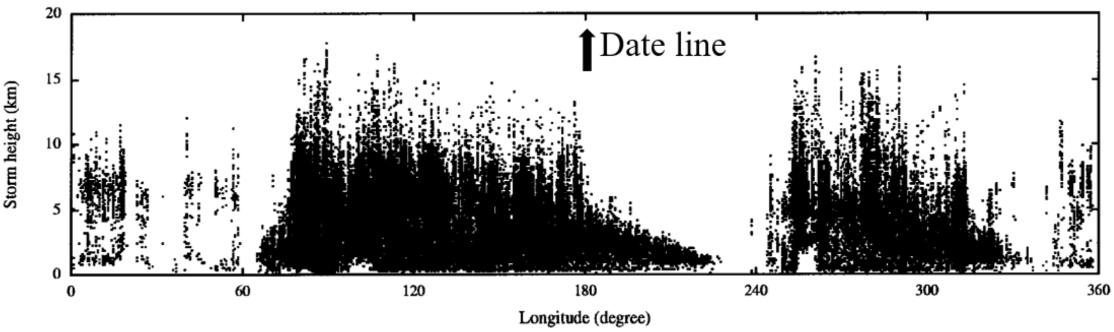

Fig. 8. Storm top distribution around 35 deg. N in summer 1998 (JAXA 2018).

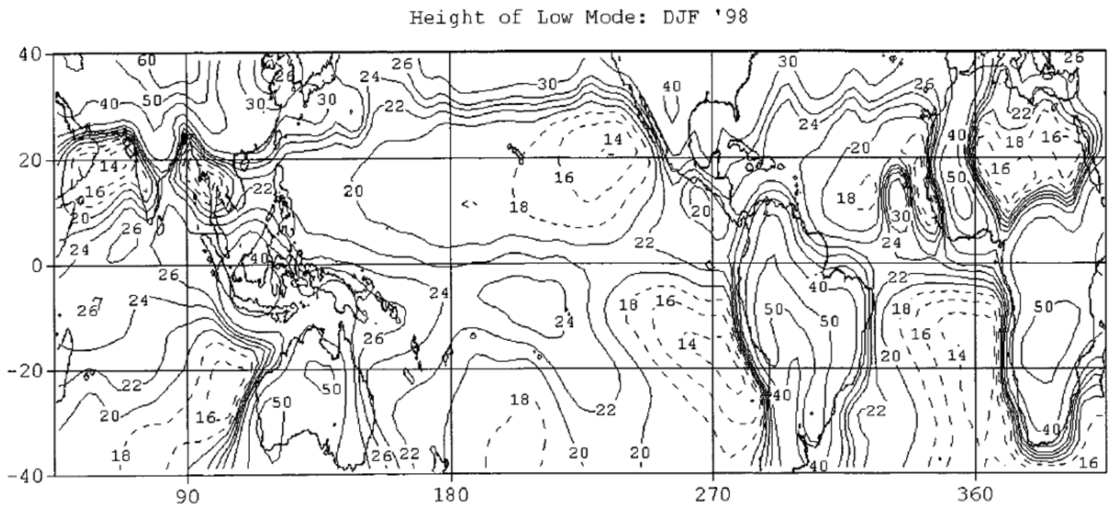

Fig. 9. Storm top distribution in DJF 1998 (Short and Nakamura 2000). (© American Meteorological Society. Used with permission)

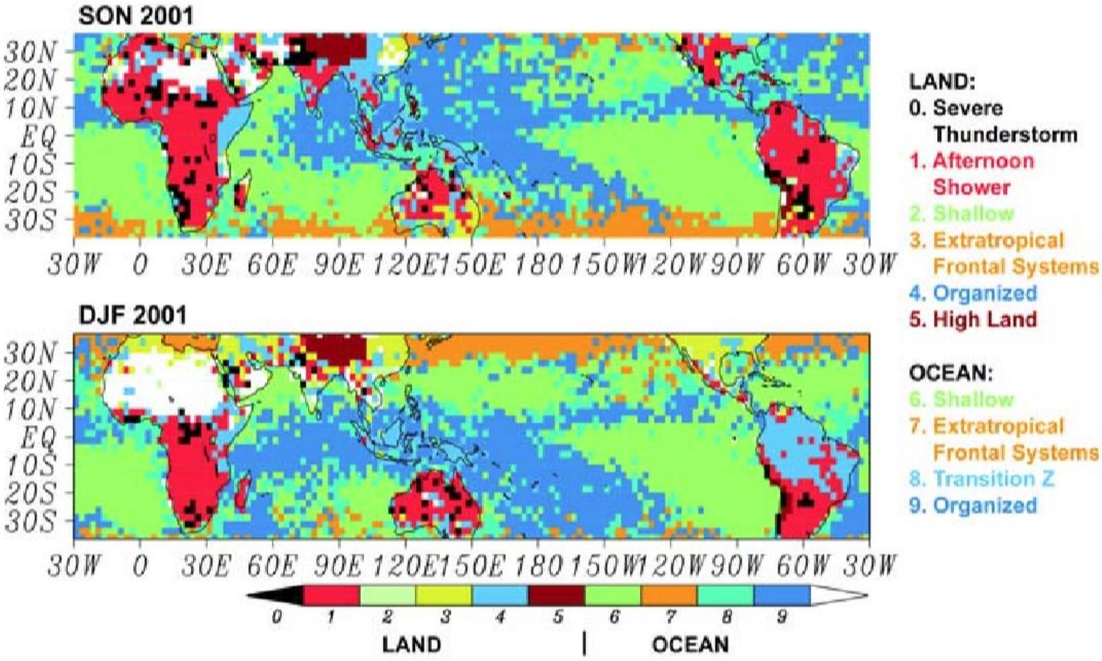

Fig. 10. Dominant precipitations derived from TRMM PR data (Takayabu 2008)

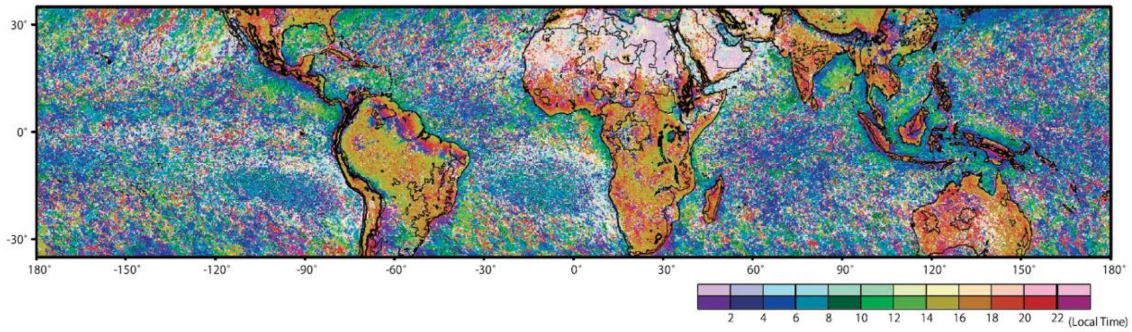

Fig. 11. Global map of peak local time of precipitation for 1998-2005 derived from TRMM microwave radiometer (TMI) (Hirose et al. 2008). (© American Meteorological Society. Used with permission)

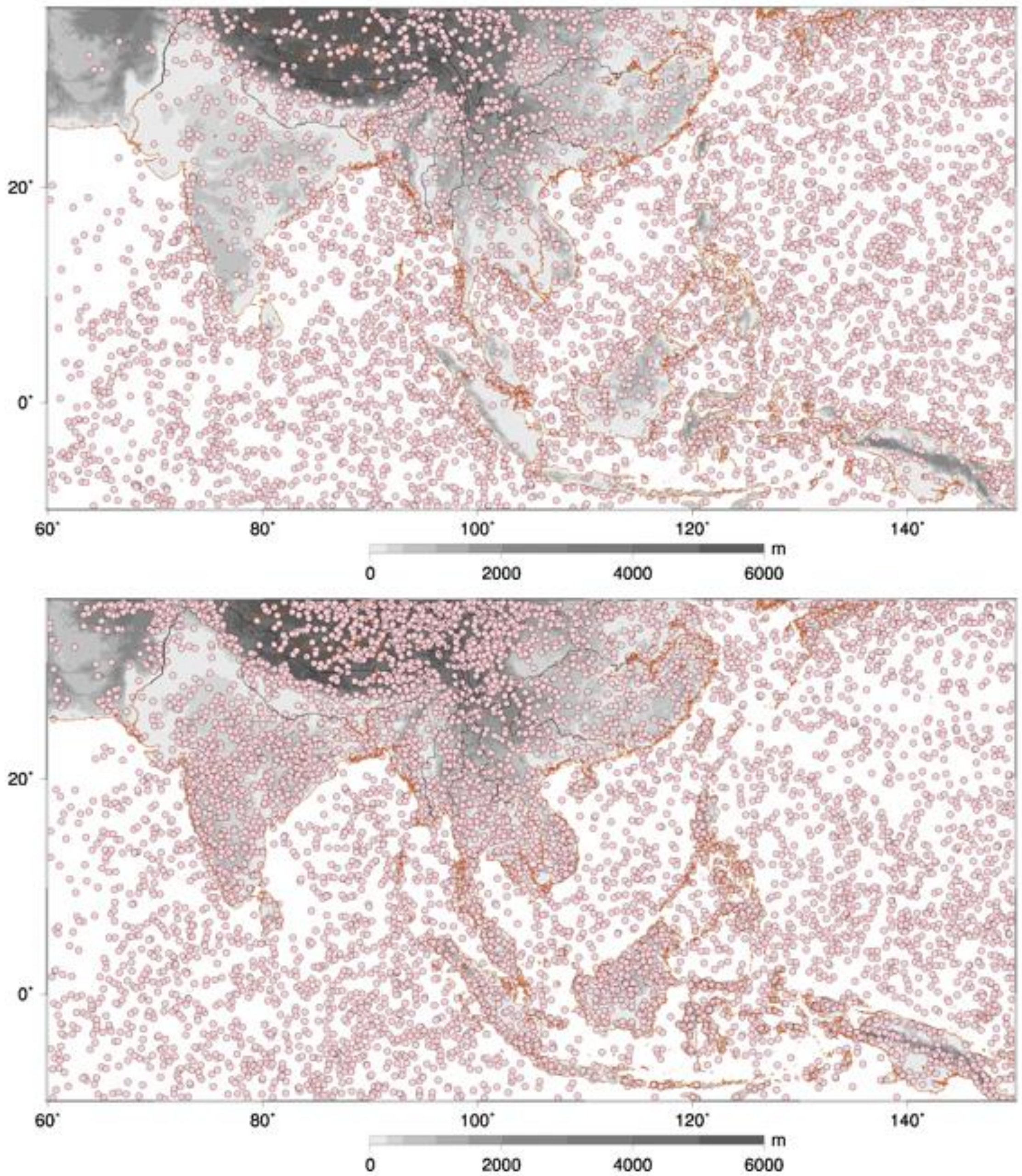

Fig. 12. Distribution of precipitation systems of 1000 – 10000 km^2 at local time of 09:00 (top) and 15:00 (bottom) in Southeast Asia in JJA for 1998 – 2003 derived from TRMM PR data (courtesy of M. Hirose, for more details, see Hirose and Nakamura 2005).

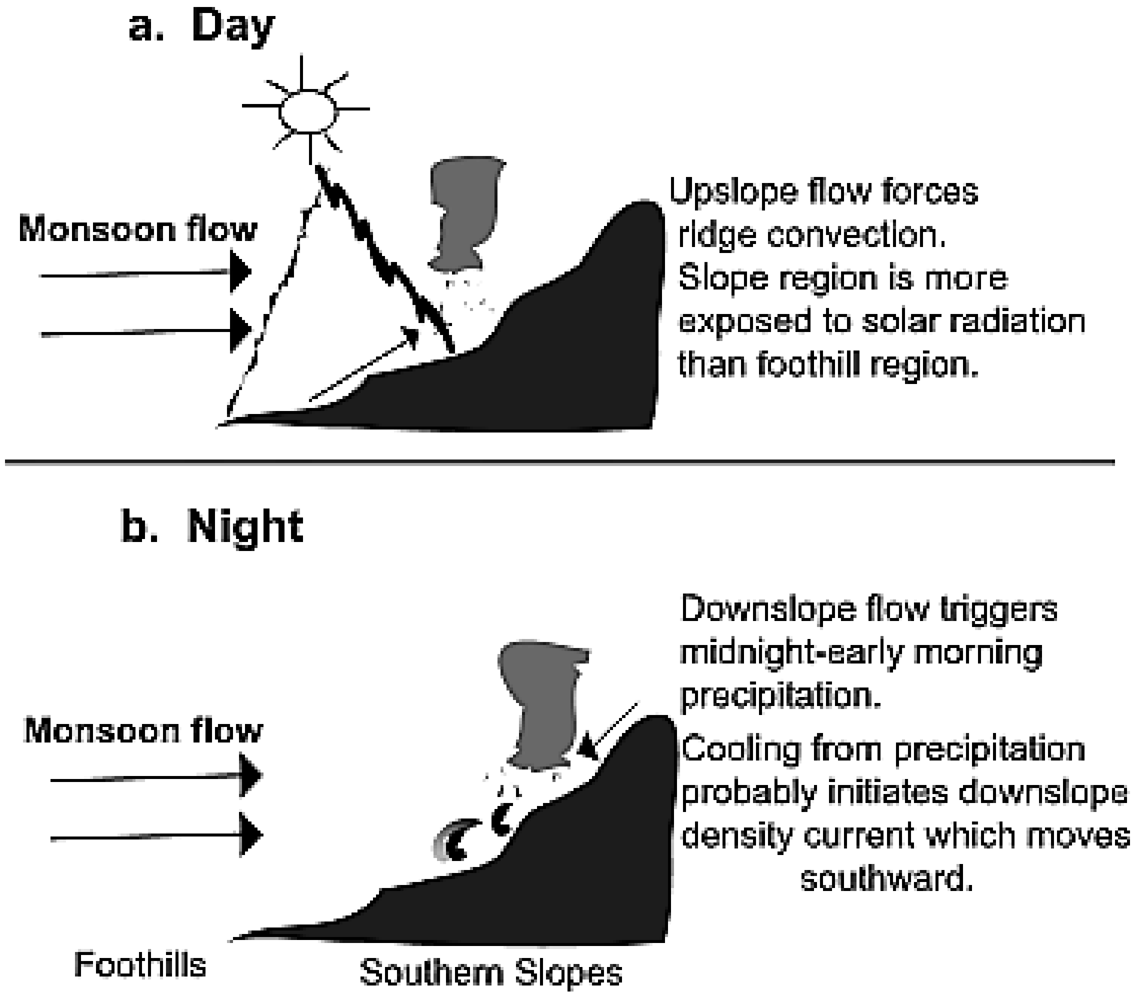

Fig. 13. Diurnal variation of precipitation over the southern slope of the Himalayas (Bhatt and Nakamura 2006).

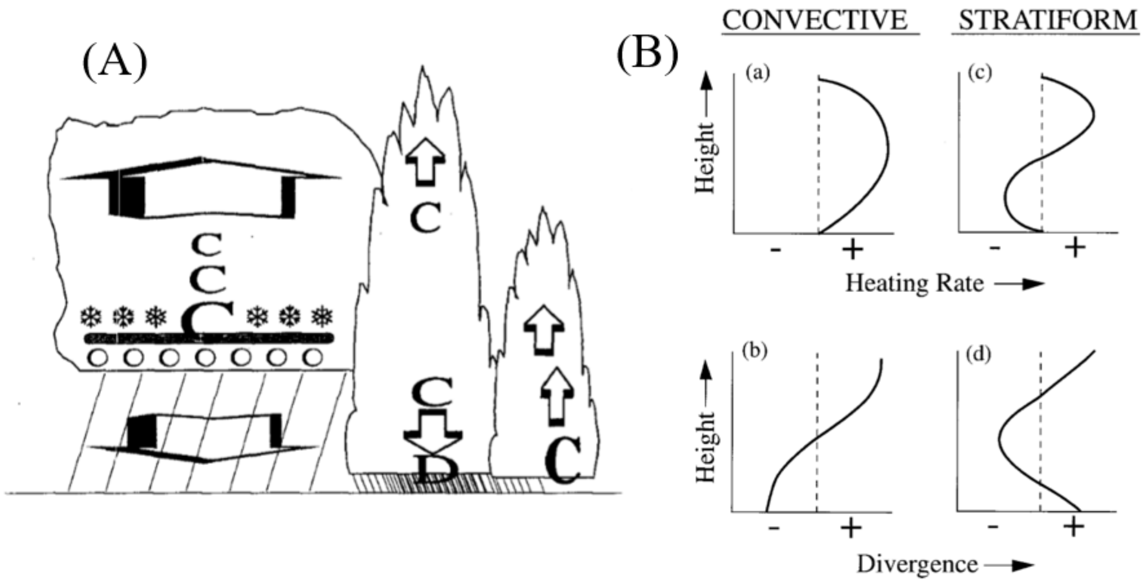

Fig. 14. Left (A): convergence and vertical air flow derived from TOGA/COARE (Mapes and Houze 1995), and right (B): latent heating profiles suggested from the field experiment like TOGA/COARE (Houze 1995). (a) and (b) are heating rate and divergence for convective, and (c) and (d) are for stratiform. (© American Meteorological Society. Used with permission)

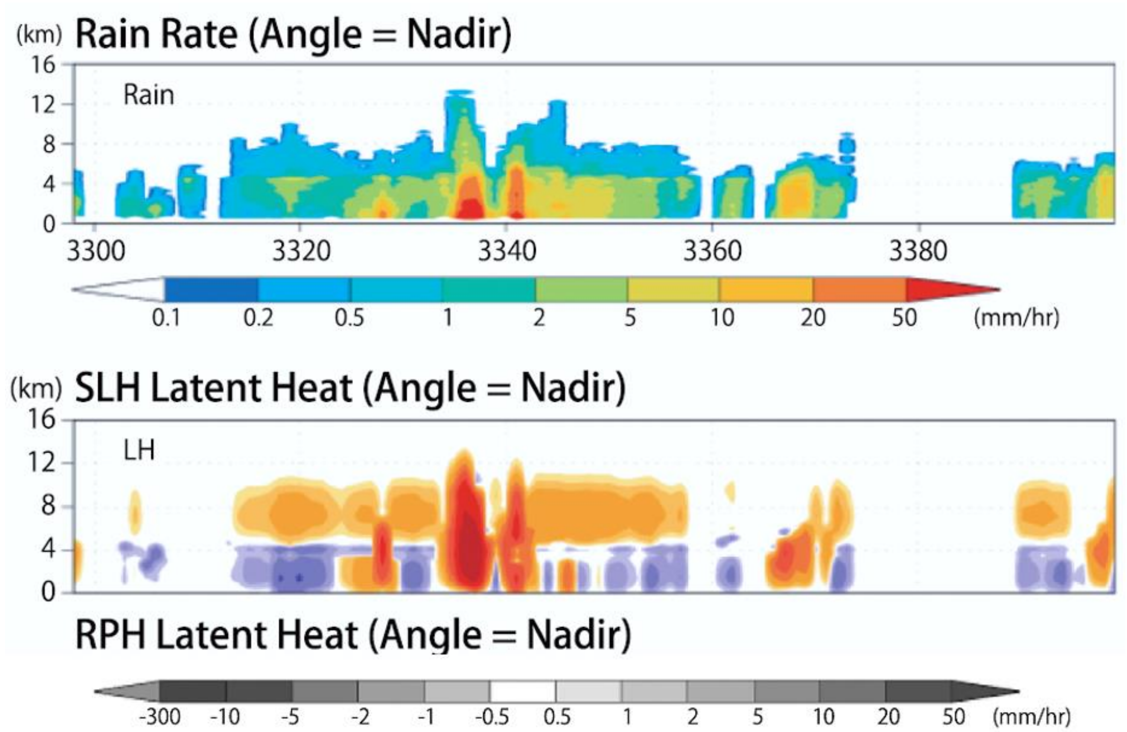

Fig. 15. Vertical cross section of rain rate (upper) and latent heat release (lower) for a typhoon (JAXA 2018).

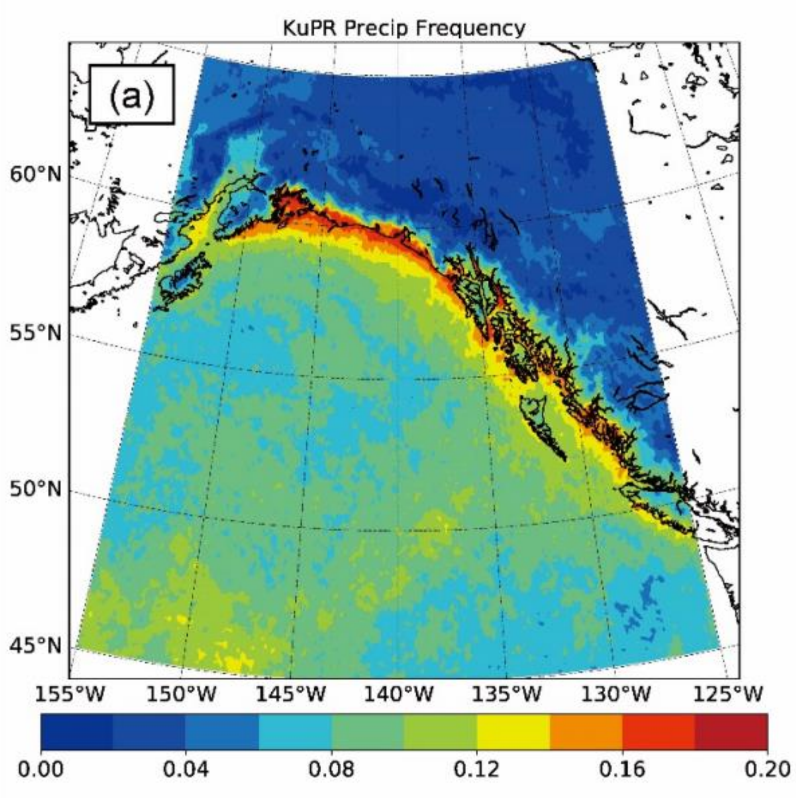

Fig. 16. Top: five-year-mean KuPR precipitation frequency in western side of North America from April 2014 to March 2019 (Aoki and Shige 2021).

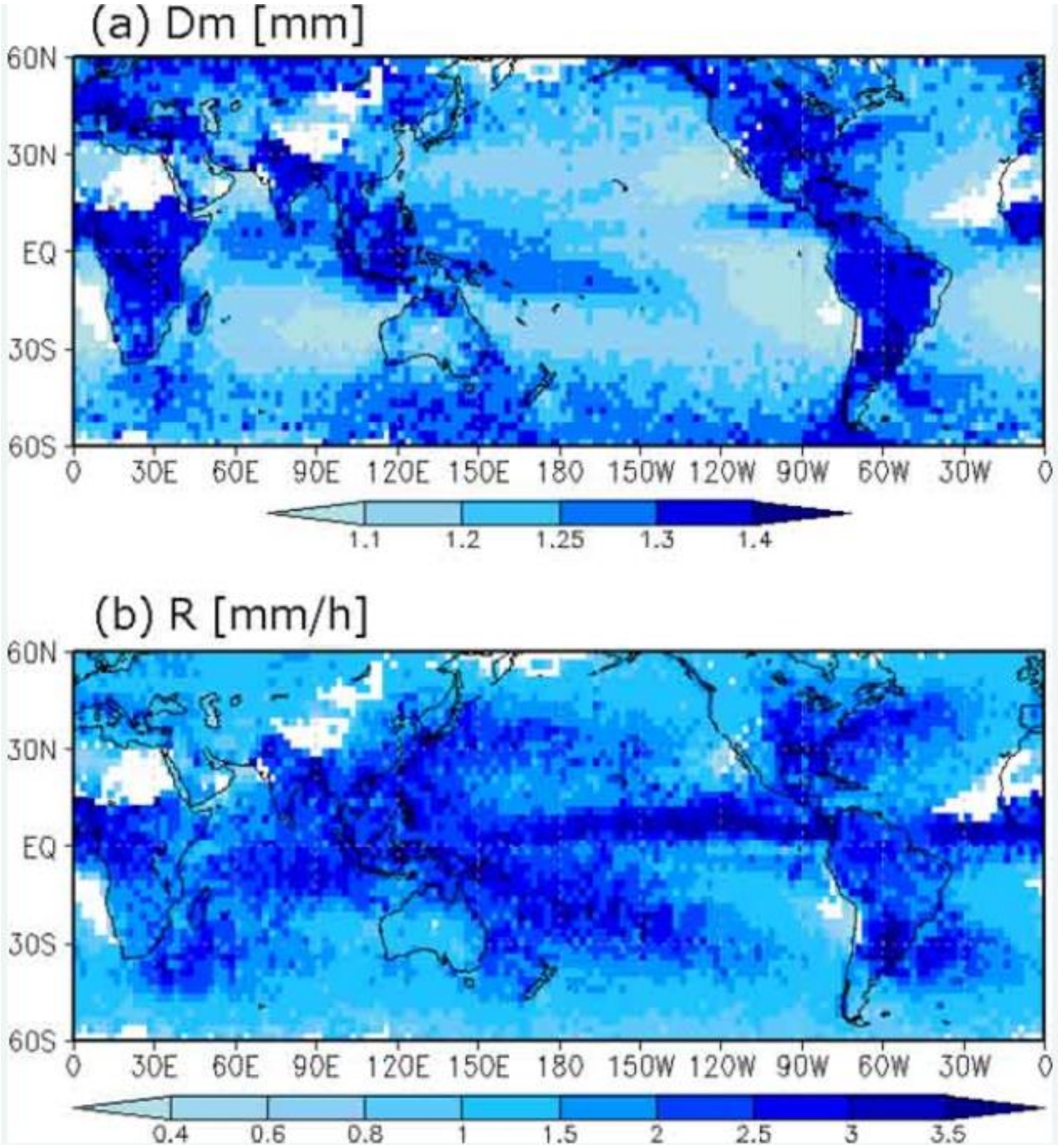

Fig. 17. Mass-weighted mean raindrop diameter (a) and mean precipitation rate rate (b) from GPM DPR 4-year data (Yamaji et al. 2020).

List of Tables

Table 1

Major characteristics of TRMM and GPM core observatory (https://www.eorc.jaxa.jp/TRMM/about/outline/outline_e.htm, https://www.wmo-sat.info/oscar/satellites/view/156).

	TRMM	GPM core observatory
Orbit altitude (km)	350, 404 (after Aug. 2001)	407
Orbit inclination (deg)	35	65
Dry mass (ton)	2.6	3.9
Electric power (W)	850 (average)	1,950 (average)
Instruments	PR, TMI, PR, VIRS, LIS, CERES	DPR, GMI
Launch date	Nov. 1997	Feb. 2014
Launcher	H-II	H-IIA

Table 2 Specifications of TRMM PR, KuPR and KaPR onboard the GPM core observatory (Hou et al. 2014, Kojima et al. 2012).

	TRMM PR	GPM KuPR	GPM KaPR
Radar type	Pulse	Pulse	Pulse
Antenna type	Active phased array	Active phased array	Active phased array
Size (m)	2.2 x 2.2	2.4 x 2.4	1.44 x 1.07
Frequency (GHz) (two frequency agility)	13.8	13.6	35.5
Swath (km)	215 245 (after Aug. 2001)	245	125
Horizontal resolution at nadir (km)	4.3 5 (after Aug. 2001)	5	5
Range resolution (m)	250	250	250/500
Transmitting peak power (W)	> 500	>1013	>146
Observation range from surface (km)	15	19	19
Detectable rain (mm h^{-1})	0.7	0.5	0.2
Mass (kg)	<465	<365	<300
Power consumption (W)	<250	<383	<297